UCRL-92510
PREPRINT

STELLAR CORE COLLAPSE AND SUPERNOVA

J. R. Wilson
R. Mayle
S. E. Woosley
T. Weaver

This paper was prepared for submittal to
Texas Relativistic Astrophysics Symposium XII,
Jerusalem, Israel
December 16-20, 1984

April 1985

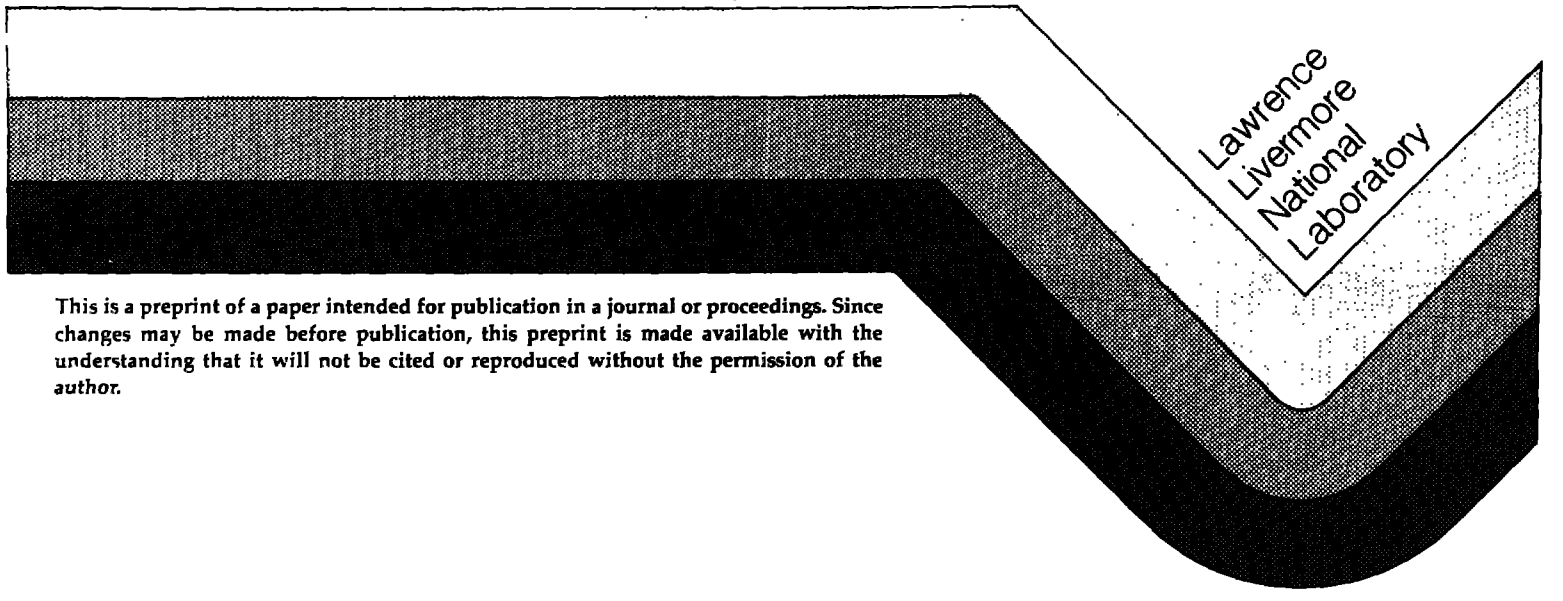

STELLAR CORE COLLAPSE AND SUPERNOVA

J. R. Wilson

Lawrence Livermore National Laboratory
Livermore, CA. 94550

R. Mayle
Physics Department
University of California
Berkeley, CA 94720
and
Lawrence Livermore National Laboratory
Livermore, CA. 94550

S. E. Woosley
Board of Studies in Astronomy and Astrophysics, Lick Observatory
University of California, Santa Cruz, CA 95064
and
Lawrence Livermore National Laboratory
Livermore, CA. 94550

T. Weaver
Lawrence Livermore National Laboratory
Livermore, CA 94550

I. INTRODUCTION

Massive stars that end their stable evolution as their iron cores collapse to a neutron star or black hole have long been considered good candidates for producing Type II supernovae. For many years the outward propagation of the shock wave produced by the bounce of these iron cores has been studied as a possible mechanism for the explosion (cf. Bowers and Wilson 1982a; Arnett 1980, 1983; Brown, Bethe, and Baym 1982; Hillebrandt 1984; Bruenn 1984; Cooperstein 1982; Kahana, Baron, and Cooperstein 1984). For the most part, the results of these studies have not been particularly encouraging, except, perhaps, in the case of very low mass iron cores (Hillebrandt, Nomoto, and Wolff 1984; Cooperstein 1982) or very soft nuclear equations of state (Baron, Cooperstein, and Kahana 1985). The shock stalls, overwhelmed by photodisintegration and neutrino losses, and the star does not explode. More recently, slow late time heating of the envelope of the incipient neutron star has been found to be capable of rejeuvinating the stalled shock and producing an explosion after all (Wilson 1985; Bethe and Wilson 1985). The present paper discusses this late time heating and presents results from numerical calculations of the evolution, core collapse, and subsequent explosion of a number of recent stellar models. For the first time they all, except perhaps the most massive, explode with reasonable choices of input physics.

II. PRE-EXPLOSIVE MODELS

A number of presupernova stellar models were considered which varied in mass and the input physics used to study their stable evolution. Because of these variations, the iron cores at the time of collapse spanned a range of masses from 1.31 $M_\odot$ to 2.22 $M_\odot$ (Table 1). Several of these models have been published previously and the detailed evolution of the remainder is the subject of papers now in preparation.

The star of lowest main sequence mass considered here, Model 10A, was calculated by Woosley, Weaver, and Taam (1982) using the older version of the stellar evolution program KEPLER described by Weaver, Zimmerman, and Woosley (1978). In particular, the Fowler, Caughlan, and Zimmerman (1975) reaction rate for $^{12}C(\alpha,\gamma)^{16}O$ was employed as well as earlier vintages of electron capture rates, screening corrections, initial composition, and prescription for silicon burning. A similar core evolution up through the onset of degenerate neon shell flashes has recently been determined by Nomoto (1984ab) for a 2.6 $M_\odot$ helium core. In both cases the evolution is characterized by temperature inversion in the core and off-center burning. In particular, neon, oxygen, and silicon burning all ignite off-center (in the Woosley, Weaver, and Taam study) and the hydrogen and helium shells are ejected by a particularly violent neon flash roughly 5 years before the star explodes. Previous studies of

core bounce in this star have shown no prompt hydrodynamical explosion (Bowers and Wilson 1982a; Bruenn 1984) or else a very weak one (Hillebrandt 1982). Similarities between this star and the observed properties of the Crab Nebula, especially the lack of substantial heavy element nucleosynthesis, have been noted (Arnett 1975; Woosley, Weaver, and Taam 1980; Nomoto 1982, 1984ab; Nomoto *et al* 1982; Hillebrandt 1982) and imply that the progenitor of the Crab was a star of roughly this mass. A particularly bright light curve could be a consequence of the shock interacting with the tenuous envelope ejected just before the explosion (Weaver and Woosley 1979).

Only one other model employed in this paper was calculated using the old version of KEPLER. Model 15A is identically the 15 $M_\odot$ presupernova star published by Weaver, Zimmermann, and Woosley (1978). All other stars have been evolved using a revised version of the program (Weaver, Woosley, and Fuller 1984) which incorporates the new weak interaction rates of Fuller, Fowler, and Newman (1982ab, 1984), an improved implementation of weak processes at an earlier stage of the star's life (near oxygen core depletion), revisions to nuclear screening corrections, finer time step and zoning criteria, and Cameron (1982) initial abundances. Because of the smaller helium abundance employed in the new studies, helium core masses are smaller than in the earlier studies. For example, the new 11 $M_\odot$ star has a helium core at the end of its life of 2.4 $M_\odot$, slightly *smaller* than the helium core in the old 10 $M_\odot$ star (see above). Helium core masses in the larger stars are also reduced by about 10%. More importantly, the revised weak rates and prescription for their implementation leads to *iron* core masses that are considerably smaller than in Weaver, Zimmerman, and Woosley. Model 25A is an example with an iron core mass reduced from its 1978 value, 1.61 $M_\odot$, to 1.37 $M_\odot$ (Weaver, Woosley, and Fuller 1985).

The same revised code *and 1975 version of* $^{12}C(\alpha,\gamma)^{16}O$ were also used for Models 11A, 50A, and 100A. The 11 $M_\odot$ star had an evolution that differed markedly from all the other stars examined here, but quite similar to that reported for a 9.6 $M_\odot$ star by Nomoto (1984ab; see also Miyaji *et al* 1980). The helium core mass in the Nomoto study was 2.4 $M_\odot$, roughly the same as here *at the end of the evolution.* However, just after depletion of carbon in the center of the 11 $M_\odot$ star, the helium core mass was 2.6 $M_\odot$, hydrogen dredge-up of the helium core during off-center carbon burning accounts for the difference. In a fashion similar to Model 10A discussed above, the evolution of Model 11A is characterized by temperature inversion (owing especially to plasma neutrino losses) and off-center burning. A neon core develops (60% neon and 20% each of magnesium and oxygen) containing very nearly a Chandrasekhar mass (1.45 $M_\odot$). That this mass exceeds 1.37 $M_\odot$ marks a critical departure between the present work and that of Nomoto (1984ab). For the smaller mass, neon and subsequent burning stages never ignite (under stable conditions) whereas in Model 11A, both neon and oxgen burning do occur in a shell from about 0.6 $M_\odot$ to 1.3 $M_\odot$ (Fig. 1) and, in a second convective burning stage from 1.3 $M_\odot$ to 1.4 $M_\odot$. Thus at the end of

its life this star consists of a cold ($T \sim 5 \times 10^8$ K) central core of about 0.5 $M_\odot$ of neon surrounded by silicon and sulfur with a total mass slightly exceeding the (zero entropy) Chandrasekhar mass (Fig. 2). Further cooling then leads to the collapse of the core containing combustible nuclear fuel.

It must be acknowledged at this point that the onset of collapse in this star has not been calculated in an entirely self-consistent fashion. Electron capture reactions were not included in the calculation of neon and oxygen burning although oxygen burns at such a high density off-center here that such captures would certainly have been important, probably triggering core collapse at an earlier stage. At a density of $\sim 10^8$ g cm^{-3}, for example, capture on the products of oxygen burning (eg. $^{33}S(e^-,\nu)^{33}P$; see Woosley, Arnett, and Clayton 1972) would lead to $Y_e \sim 0.49$ reducing the zero entropy Chandrasekhar mass to 1.38 $M_\odot$ and causing the core to collapse. We do not think that the continued evolution is especially sensitive to this detail, but a self-consistent calculation would obviously be desireable. It is interesting to note that the contraction of the core is not without nucleosynthetic import in the overlying layers. We find that the heating of the helium burning shell leads to extension of the helium convective zone into the hydrogen envelope. The mixing of protons into a super-heated helium shell has obvious and far reaching implications for r and s-process nucleosynthesis which will be discussed elsewhere.

As the core contracts to 2.5×10^{10} g cm^{-3}, oxygen burning, greatly enhanced by electron screening, ignites at a temperature of $\sim 5 \times 10^8$ K. We note that at this point the core is also hovering on the verge of general relativistic instability (Shapiro and Teukolsky 1984) because the mean adiabatic index, Γ, is so nearly equal to 4/3. Future calculations should also include post-Newtonian gravity. Owing to the extremely degenerate nature of the core the nuclear runaway that ensues leads to complete combustion to iron group nuclei. Here the evolution becomes quite similar to that described by Nomoto (1984ab) for the 2.4 $M_\odot$ helium core. Iron group products capture electrons efficiently leading to a sudden drop in Y_e at the center of the star to about 0.40. The thermal increment to the pressure from burning is inconsequential compared to the great loss in electron degeneracy pressure and the core begins to implode dynamically. As first neon and magnesium and, later, silicon and sulfur, fall down they are heated by compression and burn explosively so that a standing combustion front exists at $\sim$110 to 170 km. Once the collapse is well under way, energy transport by convection is negligible.

Models 12C, 15C, and 25C also used the improved version of KEPLER but incorporated additional revisions to the rate for $^{12}C(\alpha,\gamma)^{16}O$. Recent measurements by Kettner et al (1982) and reanalysis of new and old data by Langanke and Koonin (1984) have led to a revised rate, as tabulated by Caughlan et al (1984), that under typical conditions in massive stars, is about 3 times the old value used in all other calculations (Fowler, Caughlan, and Zimmerman 1975). Such a large revision has, as we shall see, major implications not only for nucleosynthesis, but also for the structure

of the presupernova star. The iron core mass in Models 12C and 15C are not greatly altered say, from Model 25A, or from the $20M_0$ star studied by Weaver, Woosley, and Fuller (1984), (although, as it turns out, the extent of the oxygen burning shell is much larger with the new rate). But Model 25C has a much larger iron core. To examine the dependence on ^{12}C (α, γ)^{16}O, a third 25 M_0 star was also studied in which the old FCZ75 rate was simply multiplied by a constant factor, 2.5. The iron core mass has an intermediate value (Table 1).

Why should there be such a great variation in the iron core mass for stars of 15 and 25 M_0 and for two stars, both of 25 M_0, differing only in the magnitude of the reaction rate for ^{12}C (α, γ)^{16}O? Models 15C and 25C, for example, which utilize otherwise identical physics including electron capture rates, have iron core masses at collapse that differ by about 0.6 M_0(Table 1). A comparable difference characterizes Models 25A and 25C. Why is the evolution so radically altered? The answer apparently resides in the nature of carbon and neon burning and how they affect the entropy structure of the stellar core. In Model 15C and Model 25A (the 25 M_0 star with low α rate) carbon burning ignites as a well developed, exoergic, convective burning stage. In fact, the $15M_0$ star goes through three distinct stages of carbon convective burning before igniting neon burning at its center. The first stage depletes carbon in a region out to about 0.4 M_0, the second convective shell goes from ~0.4 out to 1.0 M_0, and finally a third stage burns carbon out to about 1.5 M_0. The initial carbon abundance following helium burning in this star is 0.14. While carbon burning goes on, neutrino losses cool the core. During the first carbon convective stage, the central conditions are $T_c = 8.2 \times 10^8$ K, $\rho_c = 3.8 \times 10^5$ g cm^{-3} while at the end of the third stage, (at neon ignition) $T_c = 1.6 \times 10^9$ K, $\rho_c = 9.2 \times 10^6$ g cm^{-3}. This loss of entropy from the core allows it to become sufficiently degenerate that the core size becomes approximately equal to the Chandrasekhar mass. Thus a strong carbon burning shell is established at the edge of a (semi-) degenerate core. From this point onwards, there exists a sharp increase in the entropy at $M \sim 1.5$ M_0 that restrains the outward extension of convective shells during oxygen and silicon burning so that when the star finally collapses it does so with an iron core of 1.33 M_0, close to the traditional Chandrasekhar mass for material with equal numbers of neutrons and protons. At least a portion of the decrease from ~1.5 to 1.33 M_0 is a consequence of electron capture during and shortly after oxygen burning.

The 25 M_0 star with the most recent α-capture rate is quite another story. Because the carbon abundance following helium depletion is so low, ~9% by mass, carbon burning and, as it turns out, neon burning as well, never ignite in the center of the star as exoergic, convective burning stages. The trace abundances of carbon and neon burn away radiatively, without the nuclear energy generation ever exceeding neutrino losses. Because there is no cooling stage, and because the 25 M_0 star had a larger entropy in its core to start with, the core does not become especially degenerate and so

is not sensitive to the Chandrasekhar mass. Carbon is depleted radiatively out to a mass of about 2.5 $M_\odot$. Neon burns radiatively out to about 1.5 $M_\odot$. Thus the next fully developed burning stage after helium burning is oxygen burning. Prior to silicon core ignition, oxygen burns in a convective core first out to about 1.35 $M_\odot$ and then in a convective shell out to 2.4 $M_\odot$. When silicon does ignite, it is within a 2.4 $M_\odot$ core comprised of almost pure silicon and sulfur. The large entropy increase associated with the oxygen shell is then at 2.4, not 1.4 $M_\odot$ as it was in the 15 $M_\odot$ model. Silicon burns out to 1.3 $M_\odot$ but, even with $Y_e \sim 0.46$, the core is too small to collapse given its thermal content. Thus a silicon convective shell burns out to 2.2 $M_\odot$ before the core collapses.

It is interesting that the property of a massive star that most sensitively determines its final evolutionary state, neutron star or black hole, namely the iron core mass at collapse, is so sensitive to occurences in the relatively early life of the star. The 50 and 100 $M_\odot$ models used here both had old (smaller) α-capture rates and the iron core masses are expected to be even larger, with revised rates, than in Model 25C. Studies since the meeting confirm this. A new 50 $M_\odot$ model with revised alpha-rate collapses with an iron core mass of 2.4 $M_\odot$. The final value for a 100 $M_\odot$ star is expected to be even larger.

Since the baryon mass remaining after the delayed explosion always exceeds the initial iron core mass, it appears that the compact remnants of stars having main sequence mass $\gtrsim$ 20 $M_\odot$ (with exact value sensitive to $^{12}C(\alpha,\gamma)^{16}O$) will have quite different properties from those of lower mass. In particular, since nuclear equations of state suggest an upper bound to the mass of a stable neutron star of $\sim$2.0 $M_\odot$, stars heavier than $\sim 25\,M_\odot$ may leave black holes and lighter stars (but heavier than $\sim$ 8 $M_\odot$) will leave neutron stars. It is important also to note that an object which eventually, after cooling and deleptonization, becomes a black hole may be the residual of an explosion which ejects matter, produces explosive nucleosynthesis, and exhibits a light curve not markedly discrepant with observations of Type II supernovae.

III. CORE COLLAPSE AND SLOW EXPLOSION

Core collapse is initiated in all models, except 11A, by a combination of electron capture and photodisintegration (Fig. 3 and 4). Generally speaking, photodisintegration is the dominant mechanism leading to instability although in the very center of the star capture may contribute. As the collapse commences, most of the iron core falls in as a unit, *i.e.*, homologously, but as the density increases the pressure does not rise as rapidly as density to the 4/3 power. Hence a smaller and smaller fraction of the core collapses as a unit. Taking Model 25C as prototypical, just before nuclear density is achieved at the center, the sonic point is located at a mass point 0.55 $M_\odot$ so that

only 0.5 to 0.6 $M_\odot$ is collapsing homologously. After the central part of the core rises above nuclear density, the pressure rapidly increases and halts the infall of the inner 0.5 $M_\odot$ of the core. As the pressure wave moves out through the more slowly falling material a shock wave first arises at about 0.7 to 0.8 $M_\odot$. The outward propagation of this shock wave through the star has been investigated extensively over the last few years. Only in the case of very low core masses has the shock proceeded outwards with adequate energy to be considered the basis of the supernova phenomenon (Hillebrandt, Nomoto, and Wolff 1984). The success or failure of the shock in escaping the iron core depends upon subtle effects in the equation of state and neutrino cooling.

In this paper we consider the subsequent behavior of the stellar cores in models in which the shock initially fails to produce a supernova. A few hundredths of a second following bounce matter from the outer parts of the core and the surrounding stellar mantle are falling nearly freely onto an almost stationary accretion shock. Below the shock matter settles inward relatively slowly and accumulates on the dense core (Fig. 5). Consider the energy budget of the slowly settling matter at a radius $r \sim 10^7$ cm. Since the region of interest is outside the neutrinosphere, the heating by the hot radiating core is approximately

$$\begin{aligned} \dot{E}_+ &= \kappa_a(T_p)\ (L_\nu Y_n\ + L_{\bar{\nu}} Y_p)/4\pi r^2 \\ &\approx \kappa_a(T_p)\ L_\nu/4\pi r^2 \end{aligned} \tag{1}$$

where $L_\nu \approx L_{\bar{\nu}}$ at late times and matter is presumed to be dissociated into free nucleons in the region of interest. Here κ_a is the absorption opacity, T_p, the neutrinosphere temperature, L_ν, the electron neutrino luminosity, and r, the radius. Heating due to electron scattering is initially small and is ignored here. The cooling rate of the matter on the other hand is

$$\dot{E}_- = \kappa_e(T_m) a' c T_m^4 \tag{2}$$

where κ_e is the emmision opacity, T_m, the local matter temperature, and a' is the radiation constant for neutrinos ($\frac{7}{16}$ of the photon radiation constant).

The matter in the region of interest is only moderately degenerate. For this case

$$\begin{aligned} \kappa_a &= 1.33\ \sigma_0 (\frac{\epsilon_\nu}{m_e c^2})^2 / m_H \\ &\approx 11.0 \times 10^{-19} T_p^2\ cm^2\ g^{-1} \end{aligned} \tag{3}$$

where $\kappa_e = 11.0 \times 10^{-19}\ T_m^2$ and where temperatures are measured in MeV. One can also write

$$\begin{aligned} L_\gamma &= 4\pi r_p^2 a' c T_p^4/4, \\ \dot{E}_{net} &= 2.0 \times 10^{18}\ T_p^6 \left((\frac{r_p}{2r_m})^2 - (\frac{T_m}{T_p})^6 \right). \end{aligned} \tag{4}$$

Thus if $T_m < T_p (r_p/2r_m)^{1/3}$ heating of the matter will occur. For a core mass of 1.5 Mo, the gravitation energy is GE = 2 x $10^{19}/r_7$ ergs g^{-1} (r_7 is the radius in units of 10^7 cm) which is also approximately the internal energy of the material in the region of interest. The low density of matter there implies that the nuclei will disintegrate at a low temperature, about 1 to 2 MeV. This requires an energy of about 8 x 10^{18} ergs g^{-1}. If the entropy in this region is low, less than 10k the degeneracy of the electrons may be an important sink of energy, and if the entropy is high, pairs and radiation are big sinks of energy. Thus, the heat capacity of matter in this region is large and the temperatures stay moderately low. A little outside a radius of 10^7 cm matter will be in the dissociation range and may have a temperature low enough that the core radiation can heat it.

As a specific example, consider the 25 Mo model at a relevant time when T_p = 4.5 MeV, L_ν = 1.3 x 10^{53} erg s^{-1}, and E_+ = 1.2 x $10^{21}/r^2$ erg g^{-1} s^{-1}. For a core mass of 1.5 Mo, the local gravitational energy is of order 2 x $10^{19}/r_7$ erg g^{-1} s^{-1} and a characteristic heating time scale is 0.02 sec. In practice, since losses are always important, the time scale for heating is usually a few tenths of a second. Early on the scattering on electrons of neutrinos of all types contributes about 20% to heating compared to nuclear absorpton. After the heating has progressed and the matter has expanded, pairs form which help keep the temperature down and also provide more electrons for heating by scattering. The heating by scattering on pairs becomes important at late times. For a more detailed discussion of the heating process see Bethe and Wilson (1985).

After material moves below a radius of about 10^7 cm it loses pressure support and falls rapidly down onto the dense core. This accretion onto the core adds considerably to the neutrino luminosity. The luminosity associated with accretion, which is taken as the mass flux multiplied by the gravitational potential at the core, is sometimes as large as the neutrino energy flux emerging from the core itself. Heating of the matter by the neutrinos slows down the infall of matter which in turn leads to a decrease of luminosity and heating. Thus, the accretion process may and, in somes cases, does become unstable and oscillatory.

In Figure 6 we give a radius versus time plot for selected mass points. On this graph are indicated the time intervals over which particular physical processes are important and the approximate composition of the several regions. In Figure 7 the density radius profile at the end of a model calculation is presented. Note the extreme disparity between the core density and the bubble density, while the bubble and envelope densities are quite comparable.

IV. Summary of Runs

Table 1 gave a summary of the results for the 11 cases studied (the 20 $M_\odot$ model remains under study as of the time of this writing). Figures 8a-j are the corresponding radius versus time plots. For the lower range of masses (10 to 12 $M_\odot$) the shock wave moves out continuously. Note, however, that the shock wave is moving out much more slowly than matter is falling through the shock except at late times. The mantle heating and shock propagation are a continuous process. Beginning with the 15 $M_\odot$ model and all heavier models the shock does not progress monotonically in radius with time. The retreat of the shock wave leads to more matter falling onto the central core which enhances the luminosity and leads to further heating. This interplay between heating and infall is best seen in Fig. 8j and Fig. 9.

The 11 $M_\odot$ model is different from all the others. As stated earlier, this star first evolves a 2.4 $M_\odot$ He core which later becomes unstable within its inner 1.45 $M_\odot$. At the time the stellar evolution calculation was linked to the supernova code the composition consisted of a sequence of layers, 0.20 $M_\odot$ "Fe" interior to a roughly stationary deflagration front, surrounded by 0.30 $M_\odot$ of O + Ne + Mg, 0.90 $M_\odot$ of Si, and 0.05 $M_\odot$ of O + Ne + Mg. The central density at the time the two calculations were linked was 8×10^{10} g c^{-3} and the central temperature, 0.9 MeV. The iron behind the deflagration front (located at 100 to 170 km) is highly neutronized owing to its high density. The unburned layers of oxygen, neon, magnesium and silicon have very low entropy, about $0.3k$. Hillebrant, Nomoto, and Wolff (1984) found that a somewhat similar model exploded by direct propagation of the bounce shock outward. Figure 10 shows how the density profiles compare between our model and theirs. The much steeper density profile and lower core mass of Nomoto's model should increase the likelihood of a prompt explosion, but our model explodes only after a long time and only as a consequence of neutrino energy transport. Figure 11 shows the region of net neutrino heating superimposed on the radius time graph. In order to explore the dependance of the results on the calculated composition the Si region in model 11A was artificially switched to O + Ne + Mg in the hope that the energy released by nuclear burning would enhance the possibility of a prompt explosion. These changes made only a small difference in the overall behavior.

Our calculations have used the equation of state described in Bowers and Wilson (1982a, 1982b) modified to agree with the Bethe, Brown, Cooperstein and Wilson (1983) equation of state near nuclear density. With this equation of state the bounce has a very low amplitude as can be seen from Figure 8. We find that by stiffening the equation of state below nuclear density to increase the mass of the homologously collaping core and by softening the equation of state at and above nuclear density in order to increase the amplitude of the bounce, a prompt explosion follows the bounce. The changes in the equation of state we found necessary to produce immediate explosions were large, but not ridiculous. The low mass stars 10-12 $M_\odot$ will require very careful

modeling since they are on the edge between exploding by prompt shock propagation and slow neutrino heating. This is quite important because the prompt explosions are more energetic, 10^{51} ergs or more, than the slow heating explosions.

Models 25 A, B, and C provide an interesting sequence since they have widely varying "Fe" core masses inside the same total mass of star. At the time of the start of collapse, the entropies of the inner 0.5 $M_\odot$ of the three models are 1.02, 1.30 and 1.50 respectively in units of Boltzman's constant. In Figure 8 the density profiles for the three models is shown at times when the central zone has reached a density of 10^{14} g cm^{-3}. The inner cores are seen to have converged to very similar density distributions. The entropies of the inner 0.5 $M_\odot$ at this central density are 1.32, 1.62, and 1.80. The entropies have all risen about 0.30 units, but this is not enough to affect the structure of the inner core. The average lepton numbers in the central core at the beginning of collapse were 0.431, 0.438, and 0.443, but at a central density of 10^{14} g c^{-3} they had come close to being the same at a value of 0.383. The central core is about the same in the three models. The principal difference after collapse is the higher densities of matter immediately outside the core. From Figures 8f,8g, and 8h we see the time from collapse to explosion is about the same, 0.45 s. The energy of explosions of Models 25B and 25C are about the same but Model 25A's energy is low (See Table 1). The instability of the accretion process is seen in all three 25$M_\odot$ models, while at the lower mass, 15 $M_\odot$, only one model showed the instability (See Figure 8). The biggest difference in the models would be in the explosive nucleosynthesis of the ejected matter. The density of the ejected matter just outside the collapsing core is much lower in Model 25A than in Model 25C and very little of the ejecta in Model 25A is heated to a sufficiently high temperature for explosive reprocessing. Nucleosynthesis in Model 25C will be discussed in more detail in the next section.

At late times the stellar cores may become unstable to convection. In Figure 13 the entropy and electron number are shown for Model 25C at the time of neutrino heating. Between mass 1.2 $M_\odot$ and 2.1 $M_\odot$ the core has a small decrease of entropy and so is weakly unstable in the Rayleigh-Taylor sense. All the core from 0 to 2.2 $M_\odot$ is unstable by the salt finger effect due to the negative slope of the lepton number. If the core has sufficiently large initial non-radial perturbations for growth to occur in the available time, they could increase the heat flow appreciably and lead to more energetic explosions.

A weakness of the numerical model at present is that it does not include the red shift effect due to gravity. In Figure 14 we show the magnitude of the red shifts for the several models. The luminosity at the neutrinosphere is primarily a local effect and shouldn't depend on the red shift, but the luminosity should fall off with radius outside the neutrinosphere due to gravity. In addition, the cross sections will be decreased at large distances by the red shift reduction of the neutrino energy. The low mass calculations are probably realistic in this regard, but the 50 and 100 $M_\odot$ models are rather suspect.

V. MANTLE AND ENVELOPE EJECTION

i) Explosive Nucleosynthesis

The passage of the shock wave through the overlying mantle of the star, in addition to providing the impulse for its ejection, leads to high temeperatures and nuclear reactions that were followed in detail for Models 15C and 25C (Weaver and Woosley 1985). Figure 15 shows the explosive nucleosynthesis in Model 25C and nucleosynthetic results of Models 15C and 25C are both shown compared to solar abundances in Figure 16. In the case of Model 15C, the abundances ejected are almost entirely, with the obvious exception of the iron group, produced in the pre-explosive stages of evolution and merely shoved off the star by the explosion. The diminished importance of explosive nucleosynthesis, as compared, for example, to past studies (Weaver and Woosley 1980) is a consequence of both the low explosion energy and the rapid fall off of density around the core of the pre-explosive star. The large abundances of silicon through calcium are especially a result of an extensive oxygen burning convective shell just outside the core (Fig. 3).

An interesting phenomenon observed in the 15 $M_\odot$ delayed explosion was mass *reimplosion*. The explosion energy is so low that, after hydrodynamical exchange of energy occurs throughout the mantle and the mantle interacts with the envelope, a portion of the inner mantle finds itself endowed with less than the escape velocity. About 0.7 $M_\odot$ of heavy elements, including all the iron group and most of the silicon through calcium fell back onto the core. Aside from its nucleosynthetic consequences this occurence obviously has many important implications for future study, *eg.* delayed black hole formation. However, the details of this fall back are very sensitive to the energy of the explosion which we regard, at least for the time being, as highly uncertain. Such finely tuned effects may also be sensitive to the manner in which the shock wave generated in the core bounce code was coupled back into the stellar evolution code.

It is interesting to note that the energy liberated by nuclear reactions was not an inconsequential fraction of the final explosion energy, even in Model 15C where the final kinetic energy at infinity was calculated to be 2 x 10^{50} erg, 30% of which was generated by nuclear burning during shock wave passage. Because of the larger explosion energy, there was no reimplosion in the 25 $M_\odot$. This larger explosion energy, and especially the flatter density gradient near the core (Fig. 4, 12), also imply a considerable amount of explosive nucleo- synthesis. Nuclear energy generation formed an even greater fraction of the final kinetic energy at infinity. The initial shock contained roughly 10^{51} erg as calculated in the core bounce program, but the binding energy of the mantle was also about 10^{51} erg. Nuclear burning gave 4 x 10^{50} erg and the final kinetic energy was also 4 x 10^{50} erg. Thus without the energy from nuclear burning following shock wave passage this star may well have reimploded.

The final abundances for Model 25C are shown compared to the sun in Figure 16 and are in remarkable agreement. Isotopic nucleosynthesis is currently under study in the same model and preliminary results indicate that this good agreement extends to the odd-Z elements and the less abundant, neutron-rich isotopes of most of the even Z elements. Species in the silicon through calcium group, which used to be underproduced (Woosley and Weaver 1982), and in the iron group are now produced in large quantities by explosive oxygen and silicon burning. The improvement results chiefly from a more gradual density gradient surrounding the exploding core. The production of neon and magnesium, which used to be major *overproductions* has now declined to where their underproduction is actually becoming troublesome. The changes in abundances of these two elements, both produced in the pre-explosive star, is a direct consequence of the larger $^{12}C(\alpha,\gamma)^{16}O$ reaction rate and the smaller abundance of carbon after helium burning (neon and magnesium are the principal products of carbon burning). Interestingly the new reaction rate also implies that carbon does not owe its origin to massive stars.

ii. Light Curve For Model 15C

The propagation of the shock through Models 15C was also followed using KEPLER and the optical light curve calculated. In Figure 17 this light curve is compared both to previous calculations by Weaver and Woosley (1980) of a much more energetic explosion in a similar 15 $M_\odot$ star and to observations of Type II supernova 1969l. The general shape of the light curve from the delayed explosion calculated here agrees well with the observations and, if the distance to the galaxy NGC 1058 were readjusted, might agree in absolute magnitude as well. However, measuements of the photospheric velocity in this same supernova are about three to five times greater during the plateau stage than in the calculation. Thus Model 15C in particular, and perhaps all of the delayed explosions in general, are too low in energy to have been supernova 1969l. Perhaps more energetic (prompt) explosions do occur in a limited range of lower mass stars, but with an adequate frequency to explain observations like 1969l, but it seems highly unlikely that prompt hydrodynamical explosions will ever be calculated for iron core masses as great as the 2.1 $M_\odot$ which characterizes Model 25C. Then the supernova that we most commonly see may be hydrodynamical in origin, but the elements in our own bodies would attest to the success of delayed explosions.

This research has been supported by the National Science Foundation (AST 81-08509) and, at Lawrence Livermore National Laboratory, by the U.S. Department of Energy through contract number W-7405-ENG-48 and by the Institute for Geophysics and Planetary Physics (IGPP).

REFERENCES

Arnett, W. D. 1975, Ap. J., 195, 727.

_____. 1980, Ann. N.Y. Acad. Sci., 336, 366.

_____. 1983, Ap. J. Lettr., 263, L55.

Baron, E., Cooperstein, J., and Kahana, S. 1985, preprint

Bethe, H. A., and Wilson, J. R. 1985, Ap. J., in press.

Bethe, H. A. Brown, G E. Cooperstein, Jr., and Wilson, J. R. 1983, Nucl. Phys. A, A403, 507.

Bowers, R. L., and Wilson, J. R. 1982a, Ap. J., 263, 366.

_____. 1982b, Ap. J. Suppl., 50, 115.

Brown, G. E., Bethe, H. A., and Baym, G. 1982, Nucl. Phys. A, A375, 481

Bruenn, S. 1984, preprint submitted to Ap. J. Suppl.

Cameron, A. G. W. 1982, in Essays in Nuclear Astrophysics, ed. C. A. Barnes, D. D. Clayton and D. N. Schramm, (Cambridge Univ. Press: Cambridge), p. 23.

Caughlan, G. R., Fowler, W. A., Harris, M. J., and Zimmerman, B. A. 1984, Orange Aid Preprint No. 400 Kellog Lab, Cal Tech.

Ciatti, F. L., Rosino, L., and Bertola, F. 1971, Mem. Soc. Astron. Ital., 42, 163.

Cooperstein, J., 1982, PhD thesis, SUNY-Stoney Brook.

Fowler, W. A., Cauglan, G. R., and Zimmerman, B. A. 1975, Ann. Rev. Astron. and Ap., 13, 69.

Fuller, G. M., Fowler, W. A., and Newman, M. J. 1982a, Ap. J. Suppl., 48, 279.

_____. 1982b, Ap. J., 252, 715.

_____. 1985, submitted to Ap. J.

Hillebrandt, W. 1982, Astron. and Ap. Lettr., 110, L3.

Hillebrandt, W. 1984, Ann. N. Y. Acad. Sci, 422, 197.

Hillebrandt, W., Nomoto, K., and Wolff, R. G. 1984, Astron. and Ap., 133, 175.

Kahana, S., Baron, E., and Cooperstein, J. 1984, in Problems of Collapse and Numerical Relativity, ed. D. Bancel and M. Signore, (D. Reidel: Dordrecht), p. 163.

Kettner, K. U., Becker, H. W., Buchmann, L., Gorres, J. Krawinkel, H., Rolfs, C., Schmalbrock, P., Trautvetter, H. P., and Vlieks, A. 1982, Z. Phys., A308, 73.

Kirshner, R. P., Oke, J. B., Penston, M. V., and Searle, L. 1973, Ap. J., 185, 303.

Langangke, K. and Koonin, S. 1984, preprint MAP-56, Kellogg Radiation Lab., Cal Tech, submitted to Nucl. Phys. A.

Miyaji, S., Nomoto, K., Yokoi, K., and Sugimoto, D. 1980, Publ. Astron. Soc. Japan, 32, 303.

Nomoto, K. 1982, in Supernovae: A Survey of Current Research, ed. M. J. Rees and R. J. Stoneham, (D. Reidel: Dordrecht), P. 205.

_____. 1984a, in Stellar Nucleosynthesis, ed. C. Chiosi and A. Renzini, (D. Reidel: Dordrecht), p. 239.

_____. 1984b, Ap. J., 277, 791.

Nomoto, K., Sparks, W. M. Fesen, R. A., Gull, T. R., Miyaji, S., and Sugimoto, D. 1982, Nature, 299, 803.

Schurmann, S. R., Arnett, W. D., and Falk, S W. (1979), Ap. J., 230, 11.

Weaver, T. A., Zimmerman, G. B., and Woosley, S. E. 1978, Ap. J., 225, 1021.

Weaver, T. A., and Woosley, S. E. 1979, Bull. Am. Astron. Soc., 11, 724.

_____. 1980, Ann. N. Y. Acad. Sci., 336, 335.

_____. 1985, Bull. Am. Astron. Soc., 16, 971.

Weaver, T. A., Woosley, S. E., and Fuller, G. M. 1985, in Numerical Astrophysics, ed. J. Centrella, J. LeBlanc, and R. Bowers, (Jones and Bartlett: Boston), p. 374.

Wilson, J. R. 1985, in Numerical Astrophysics, ed. J. Centrella, J. LeBlanc, and R. Bowers, (Jones and Bartlett: Boston), p. 422.

Woosley, S. E., Arnett, W. D., and Clayton, D. D. 1972, Ap. J., 175, 731.

Woosley, S. E., Weaver, T. A., and Taam, R. E. 1980, in Type I Supernovae, ed. J. C. Wheeler, (University of Texas: Austin), p. 96.

FIGURE CAPTIONS

Fig. 1 - Composition (a) and structure (b) of an 11 $M_\odot$ star (Model 11A) just after the off-center ignition of oxygen burning. The temperature at the base of the convective oxygen shell at this point is 1.87×10^9 K. The central density and temperature are 8.19×10^7 g cm^{-3} and 5.63×10^8 K respectively. The surface luminosity, effective temperature, and radius, all of which should not change prior to the stellar explosion, are 1.47×10^{38} erg s^{-1}, 4290 K, and 2.47×10^{13} cm. The neutrino luminosity is 1.21×10^{42} erg s^{-1}. Note scale breaks at 3.0 $M_\odot$ (a) and 4.0 $M_\odot$ (b).

Fig. 2 - Composition (a) and structure (b) of the central regions of an 11 $M_\odot$ star (Model 11A) just before the onset of collapse triggered by oxygen ignition and electron capture. The central density at this point is 7.1×10^9 g cm^{-3} (runaway will occur at 2.5×10^{10} g cm^{-3}) and the central temperature is 4.5×10^8 K. The total entropy in the inner 1.4 $M_\odot$, in dimensionless units, S/Nk, is ~0.65, the electron entropy, ~0.1. Partial mixing between the neon core and silicon shell is apparent in the region 0.4 to 0.5 $M_\odot$, brought about by the inversion of mean molecular weight. The temperature at the base of the convective helium shell, which by now has penetrated into the hydrogenic envelope, is greater than 4×10^8 K. The actual combustion region was not well resolved in the present calculation even though mesh sizes of $\lesssim 10^{-4}$ $M_\odot$ were employed in the helium burning region. Note scale breaks at 1.43 $M_\odot$ (a) and 1.44 $M_\odot$ (b).

Fig. 3 - Composition (a) and structure (b) of a 15 $M_\odot$ star (Model 15C) at the onset of core collapse (as defined by collapse velocity equals 1000 km s^{-1}). Interior to the iron core (1.33 $M_\odot$) energy is being lost due to a combination of neutrino emission from electron capture and photodisintegration. Both nuclear energy generation and neutrino losses are inherently negative there. Peaks in the nuclear energy generation, ϵ_{nuc}, are apparent at the silicon, oxygen, and helium burning shells. Also plotted are the neutrino losses due to plasma processes (ϵ_ν in the region outside the iron core). Note the rapid fall off in density just outside the iron core and the substantial abundances

of the elements silicon thru calcium in the oxygen convective shell. For the most part, the oxygen shell is ejected (in this model only) without much explosive modification.

Fig. 4 - Composition (a) and structure (b) of a 25 $M_\odot$ star (Model 25C) at the onset of core collapse. Note the large iron and the less rapid fall off in density (compared to Fig. 3) outside that iron core. Notation and sampling time are as in Fig. 3.

Fig. 5 - Schematic representation of typical conditions in a star a star a few seconds after core bounce.

Fig. 6 - Radius as a function of time for selected mass points for Model 25B. Indicated compositions are the major composition between the dashed lines. The approximate time intervals of the important processes are indicated above and below the graph.

Fig. 7 - Density as a function of radius for Model 25B at a late time, 1.05 s.

Fig. 8 - Radius as a function of time time for selected mass points for all the models of Table 1. Time on the graphs starts shortly before bounce.

Fig. 9 - Neutrino luminosity and mass accretion rate at a radius of 100 km for the 100 $M_\odot$ model. The luminosity is in units of 10^{53} erg s^{-1} and the accretion rate is in units of 10^{33} g s^{-1}.

Fig. 10 - Initial density distributions for Model 11A of the present study, I, and for Nomoto's 2.2 $M_\odot$ He core model, II, at a time near the onset of core collapse. The density profile for Nomoto's model is adopted from Hillebrandt, Nomoto, and Wolff (1984).

Fig. 11 - Radius as a function of time for select mass points in Model 11A. The region of net heating is interior to the heavy lines. The numbers inside are the

heating rates in 10^{20} erg g^{-1} s^{-1} at the positions of the numbers. The curve labeled E is the energy of matter above the escape energy.

Fig. 12 - Density as a function of enclosed mass for Models 25A, 25B, and 25C.

Fig. 13 - Dimensionless entropy, S, and lepton number, Y_L, as a function of mass for Model 25C at a time 0.86 s. This is the beginning of the explosion.

Fig. 14 - Gravitational red shifts at the neutrino photosphere as a function of the mass of several models. The top curve is the red shift at the end of the calculation. The bottom curve is the red shift at the time when the star first has some matter with energy in excess of the escape energy (the point for the 100 $M_\odot$ model was arbitrarily taken at 1 s since mass ejection was never achieved by that model).

Fig. 15 - Composition of the inner regions of a 25 $M_\odot$ supernova following shock passage and ejection. The pre-explosive composition (See Fig.4) is substantially altered out to about 3.6 $M_\odot$. Composition interior to the mass cut, 2.44 $M_\odot$, is not plotted.

Fig. 16 - Comparison of bulk elemental nucleosynthesis in 15 and 25 $M_\odot$ supernovae (Models 15C and 25C) to solar abundances (Cameron 1982). The enhancement factor is the mass fraction of a given element in the ejecta compared to its mass fraction in the sun (which was also its initial abundance in the calculation). The deficient production of carbon, neon, and magnesium, especially in the 15 $M_\odot$ study, is a consequence of the revised rate for $^{12}C(\alpha,\gamma)^{16}O$. The large productions of silicon thru calcium in the 15 $M_\odot$ model do not exist if this material falls back onto the neutron star following hydrodynamical interaction with the stellar envelope. Such was the result in the present study, but this occurence is quite model dependent.

Fig. 17 - Light curve of a 15 $M_\odot$ supernova (Model 15C) which explodes

by the delayed mechanism (solid line). The qualitative nature of the curve, including the duration of the event, are in agreement with observations of supernova 1969l but only if the distance to NGC 1058 is reduced by a factor of about 3 compared to currently accepted values. A more energetic explosion would give a brighter light curve as evidenced by the two models previously calculated by Weaver and Woosley (1980). The dashed line was an explosion characterized by total kinetic energy at infinity of 3.3×10^{51} erg. The dot-dashed line was a similar model with 1.3×10^{51} erg of kinetic energy. The expansion velocity of Model 15C is much too slow to agree with observations of 1969l (Kirshner *et al* 1973; Weaver and Woosley 1980). The experimental points are UBV Data of Ciatti, et al. (1971) as transformed by the method of Schurmann et al. (1978), and Integrated Multifrequency Scans of Kirshner et al. (1973).

Summary of Runs

Table 1

Initial Stellar Mass	Model	Initial Iron Core Mass	Explosion Energy[a]	Residual Mass In Baryons	Final Neutron Star Mass
10	A old	1.40	1.8×10^{50}	1.47	1.33
11	A	.20	3.0	1.42	1.31
12	C	1.31	3.8	1.35	1.26
15	A old	1.56	3.4	1.75	1.53
15	C	1.33	3.5	1.42	1.31
20	C	1.9	Not Run Through Collapse		
25	A old	1.37	4.5	1.66	1.46
25	B	1.63	11.0	1.83	1.58
25	C	2.22	10.	2.44	1.96 B.H.?
50	A	1.79	7.5	1.86	1.60
100	A	1.85	0	>2.95	B.H.?

MODEL = A Rate $C(\alpha,\gamma)O = 1$
B Rate $C(\alpha,\gamma)O = 2.5$
C Rate $C(\alpha,\gamma)O = 3.0$

[a]As calculated in the core bounce code for the inner mantle only. The final kinetic energy at infinity will be smaller.

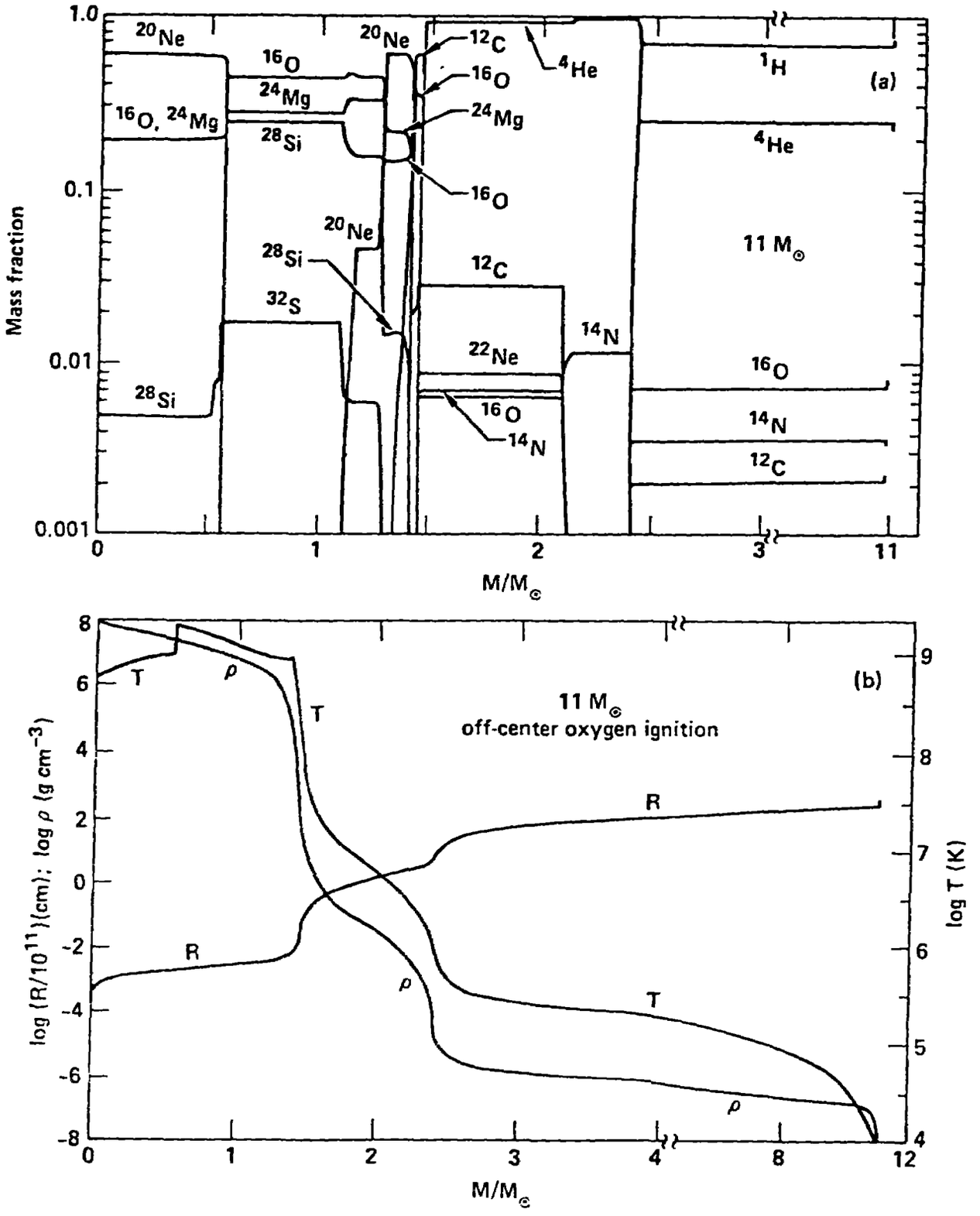
Mass fraction
1.0
0.1
0.01
0.001
^{20}Ne
^{16}O
^{24}Mg
^{16}O, ^{24}Mg
^{28}Si
^{20}Ne
^{12}C
^{4}He
^{16}O
^{24}Mg
^{16}O
^{1}H
(a)
^{4}He
11 M$_\odot$
^{20}Ne
^{28}Si
^{32}S
^{12}C
^{14}N
^{22}Ne
^{16}O
^{28}Si
^{16}O
^{14}N
^{14}N
^{12}C
0
1
2
3
11
M/M$_\odot$
8
6
4
2
0
-2
-4
-6
-8
log (R/10^{11})(cm); log ρ (g cm^{-3})
T
ρ
T
11 M$_\odot$
off-center oxygen ignition
(b)
R
R
ρ
T
ρ
9
8
7
6
5
4
log T (K)
0
1
2
3
4
8
12
M/M$_\odot$

FIG. 1

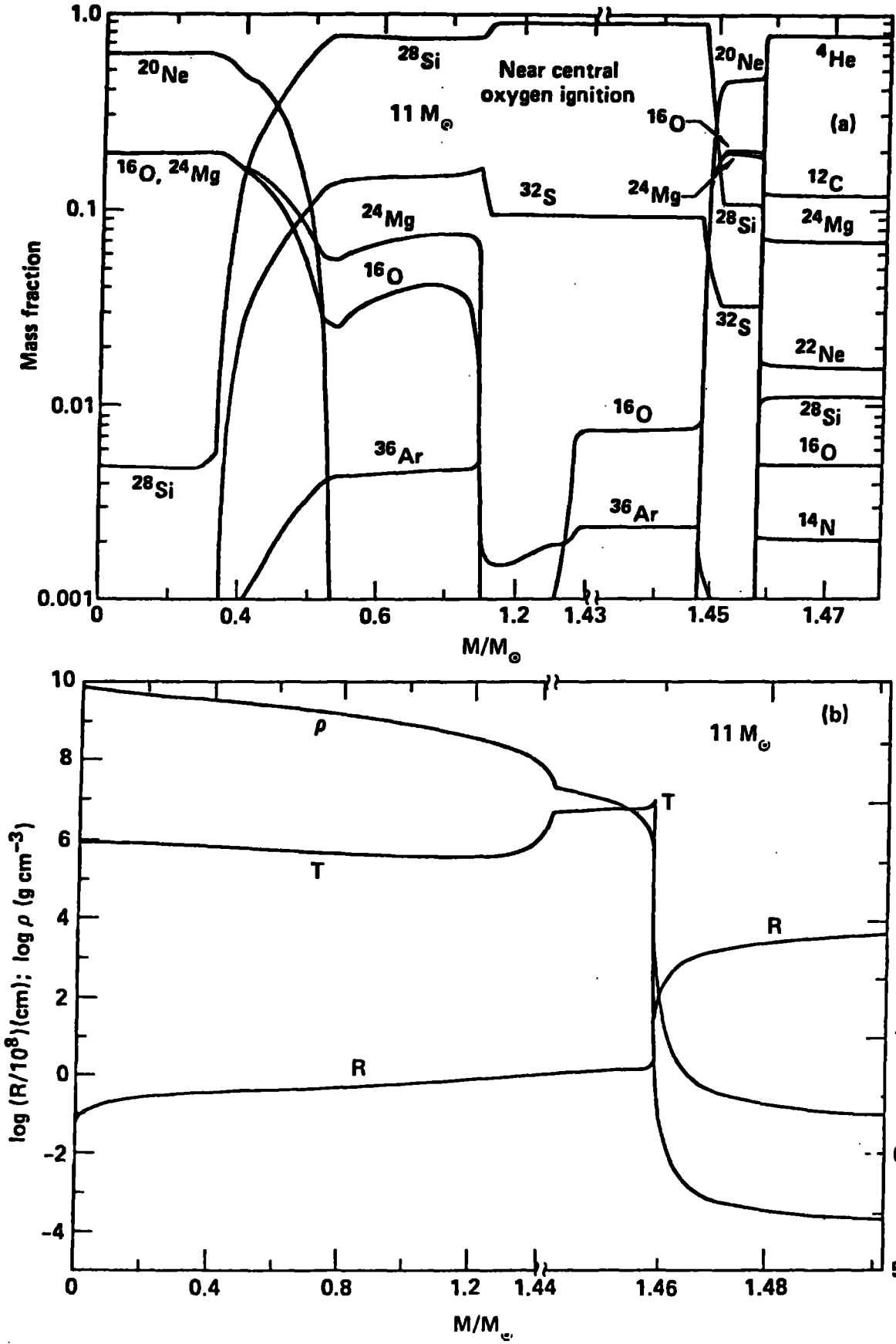
Near central
oxygen ignition
11 M⊙
(a)
20Ne
16O, 24Mg
28Si
24Mg
16O
32S
36Ar
28Si
20Ne
16O
24Mg
32S
4He
12C
24Mg
28Si
22Ne
16O
36Ar
28Si
16O
14N
Mass fraction
1.0
0.1
0.01
0.001
0
0.4
0.6
1.2
1.43
1.45
1.47
M/M⊙
(b)
11 M⊙
ρ
T
T
R
R
log (R/10^8)(cm); log ρ (g cm^-3)
log T (K)
10
8
6
4
2
0
-2
-4
9
7
5
0
0.4
0.8
1.2
1.44
1.46
1.48
M/M⊙

FIG. 2

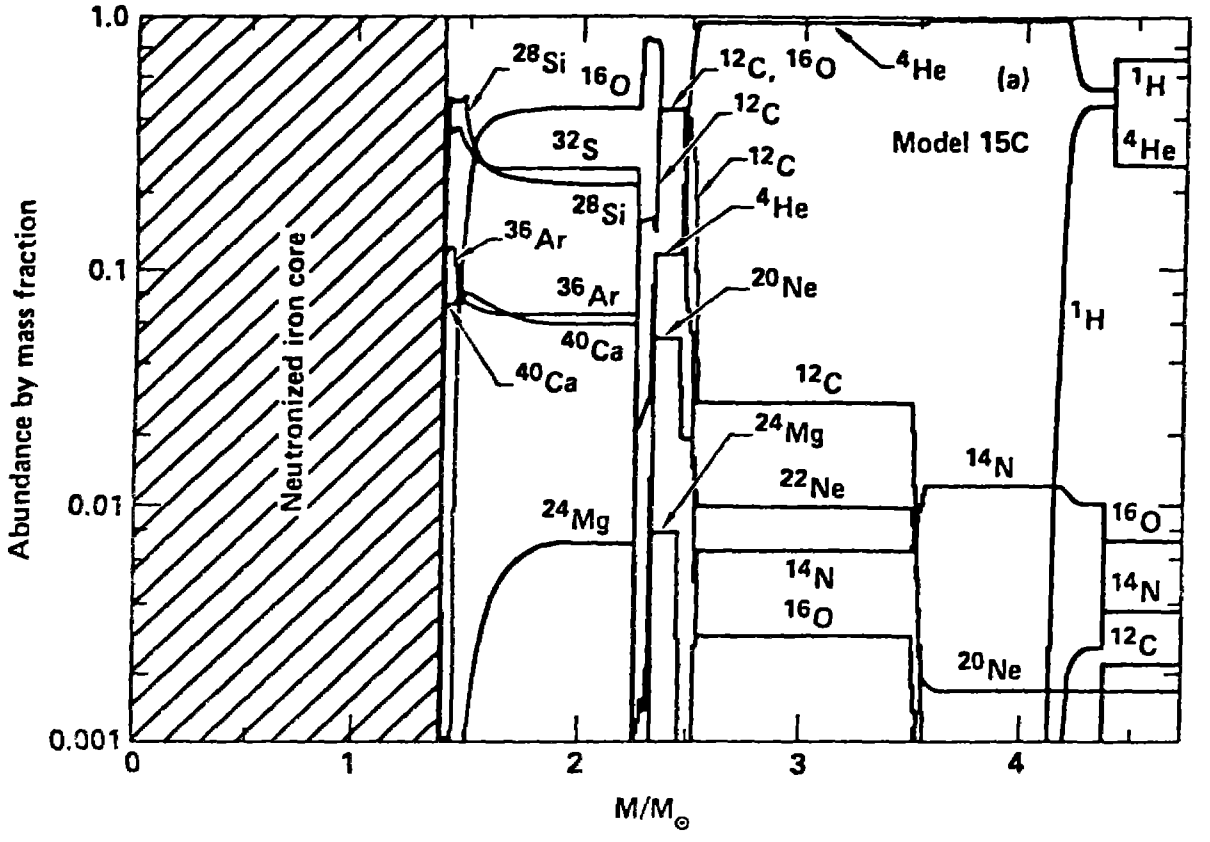
Abundance by mass fraction
1.0
0.1
0.01
0.001
Neutronized iron core
28Si
16O
12C, 16O
4He
(a)
Model 15C
1H
4He
32S
12C
12C
28Si
4He
36Ar
20Ne
36Ar
1H
40Ca
40Ca
12C
24Mg
14N
22Ne
24Mg
16O
14N
16O
14N
12C
20Ne
0
1
2
3
4
M/M⊙

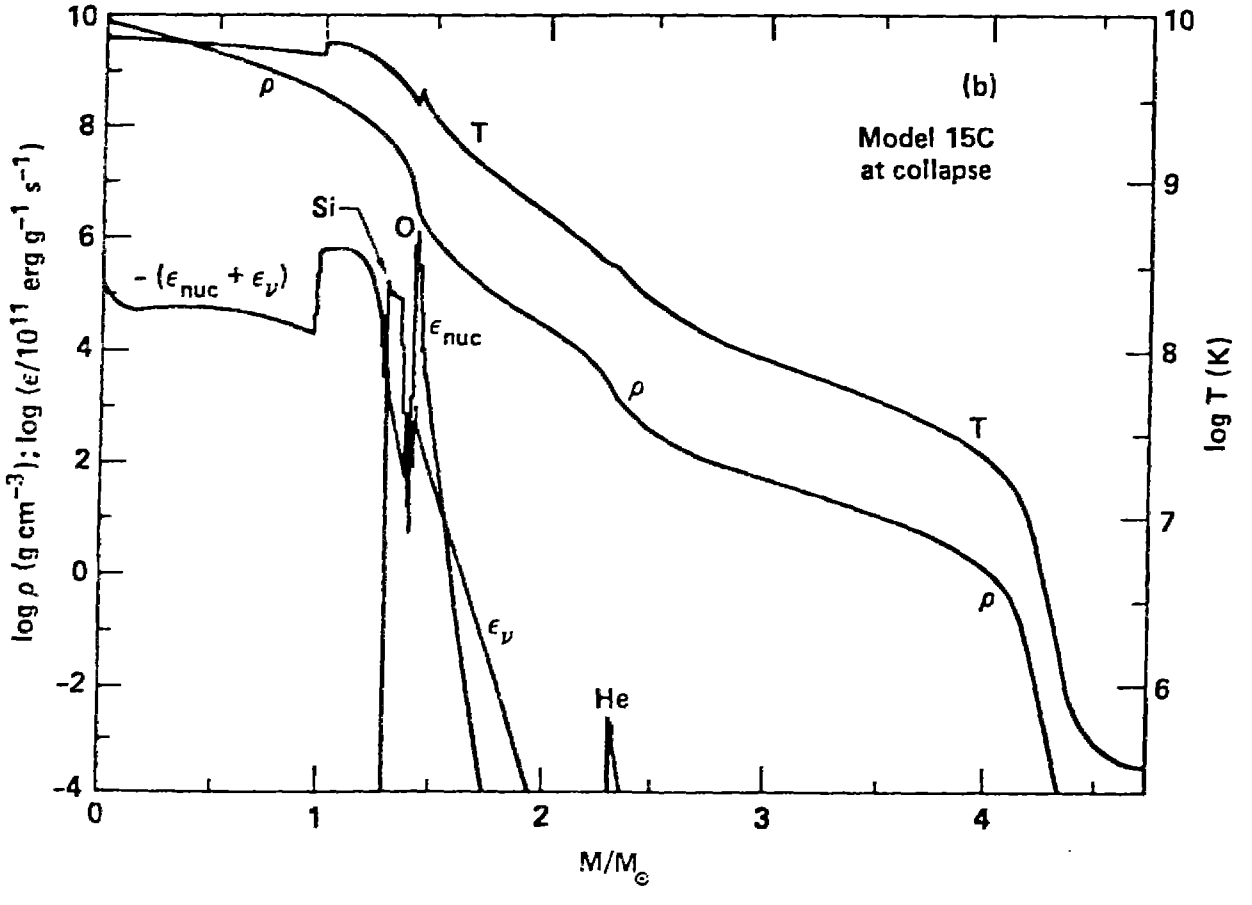
log ρ (g cm−3); log (ε/10^11 erg g−1 s−1)
log T (K)
10
8
6
4
2
0
-2
-4
9
7
6
ρ
T
(b)
Model 15C
at collapse
Si
O
-(εnuc + εν)
εnuc
ρ
T
ρ
εν
He
0
1
2
3
4
M/M⊙

FIG. 3

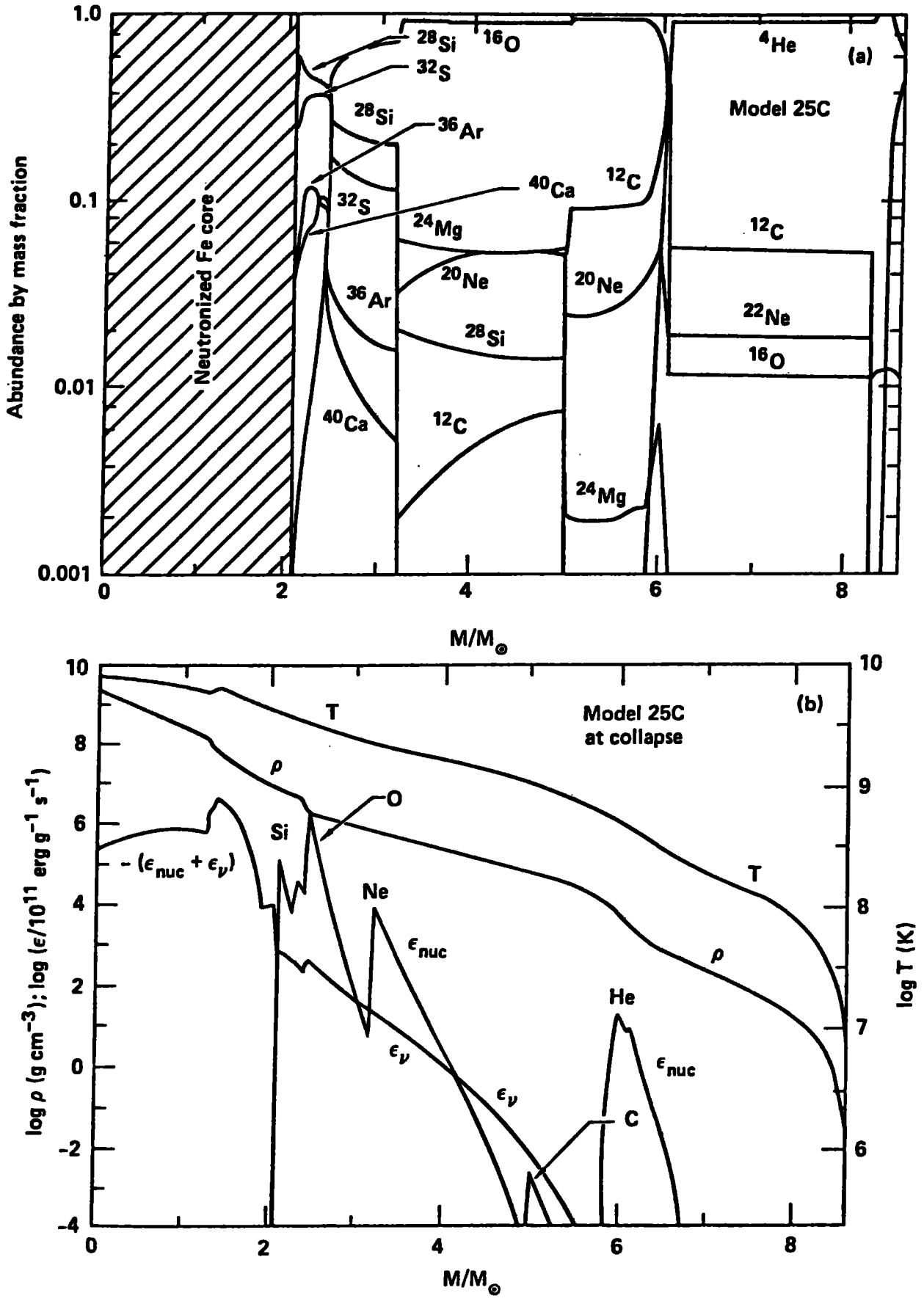
Abundance by mass fraction
1.0
0.1
0.01
0.001
Neutronized Fe core
^{28}Si
^{16}O
^{32}S
^{28}Si
^{36}Ar
^{40}Ca
^{12}C
^{32}S
^{24}Mg
^{20}Ne
^{36}Ar
^{28}Si
^{40}Ca
^{12}C
^{20}Ne
^{24}Mg
^{4}He
(a)
Model 25C
^{12}C
^{22}Ne
^{16}O
0
2
4
6
8
M/M$_\odot$
10
8
6
4
2
0
-2
-4
log ρ (g cm^{-3}); log (ε/10^{11} erg g^{-1} s^{-1})
T
ρ
O
Si
- (ε$_{nuc}$ + ε$_\nu$)
Ne
ε$_{nuc}$
ε$_\nu$
ε$_\nu$
He
ε$_{nuc}$
C
T
ρ
Model 25C
at collapse
(b)
10
9
8
7
6
log T (K)
0
2
4
6
8
M/M$_\odot$

FIG 4

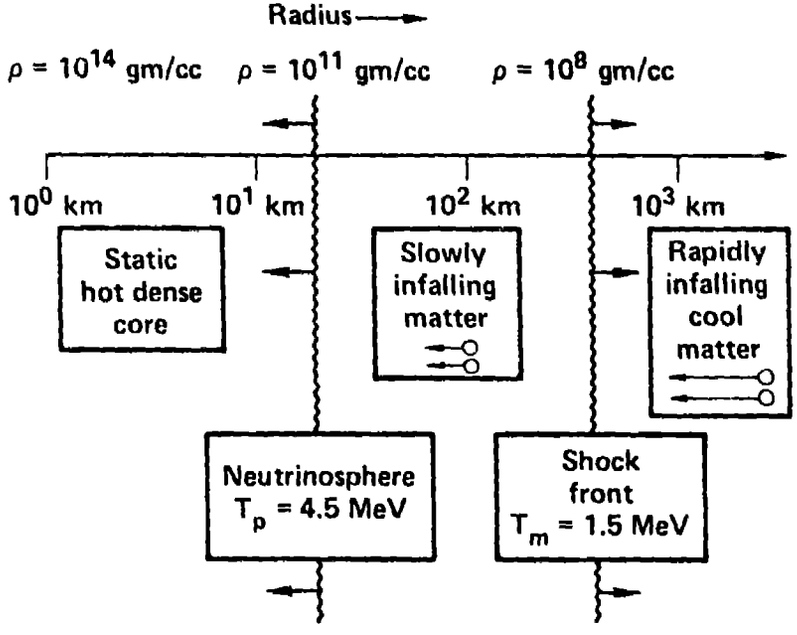
Radius
$\rho = 10^{14}$ gm/cc
$\rho = 10^{11}$ gm/cc
$\rho = 10^{8}$ gm/cc
10^0 km
10^1 km
10^2 km
10^3 km
Static hot dense core
Slowly infalling matter
Rapidly infalling cool matter
Neutrinosphere T_p = 4.5 MeV
Shock front T_m = 1.5 MeV

FIG. 5

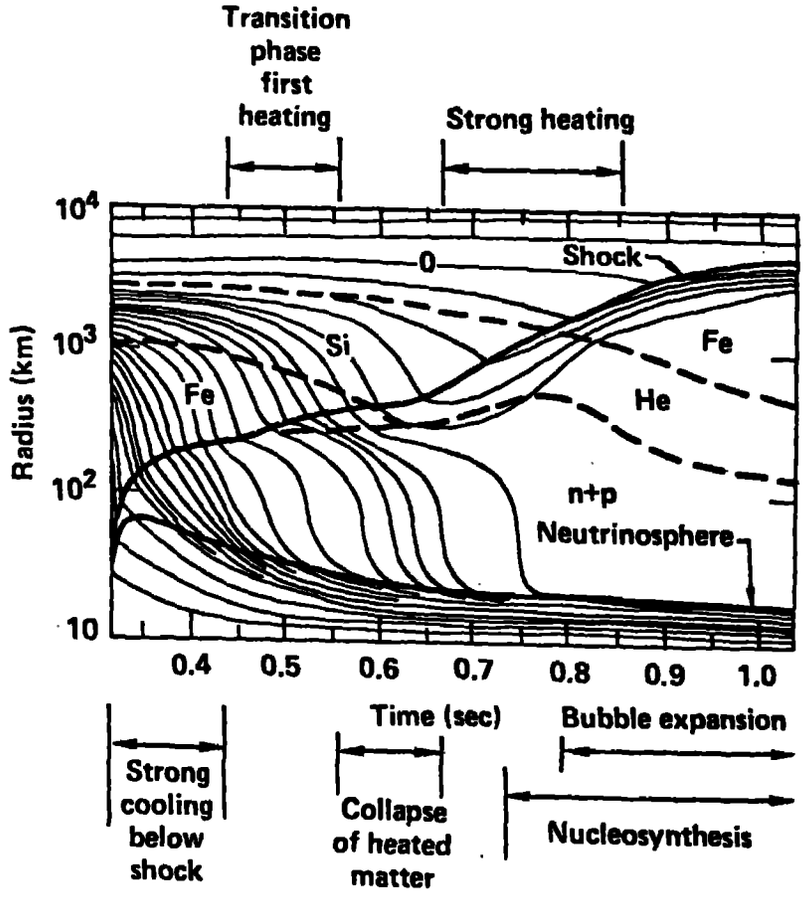
Transition phase first heating
Strong heating
10^4
10^3
10^2
10
Radius (km)
0
Shock
Si
Fe
Fe
He
n+p
Neutrinosphere
0.4
0.5
0.6
0.7
0.8
0.9
1.0
Time (sec)
Bubble expansion
Strong cooling below shock
Collapse of heated matter
Nucleosynthesis

FIG. 5

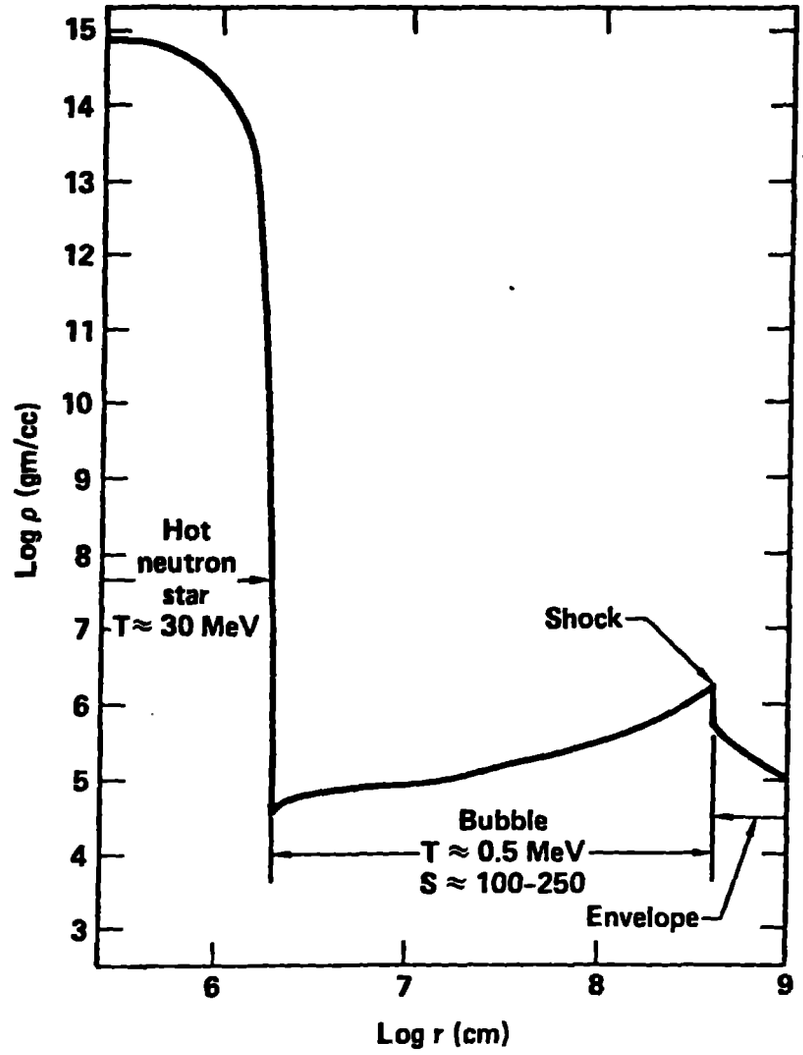
15
14
13
12
11
10
9
8
7
6
5
4
3
Log ρ (gm/cc)
Hot
neutron
star
T≈ 30 MeV
Shock
Bubble
T ≈ 0.5 MeV
S ≈ 100-250
Envelope
6
7
8
9
Log r (cm)

FIG. 7

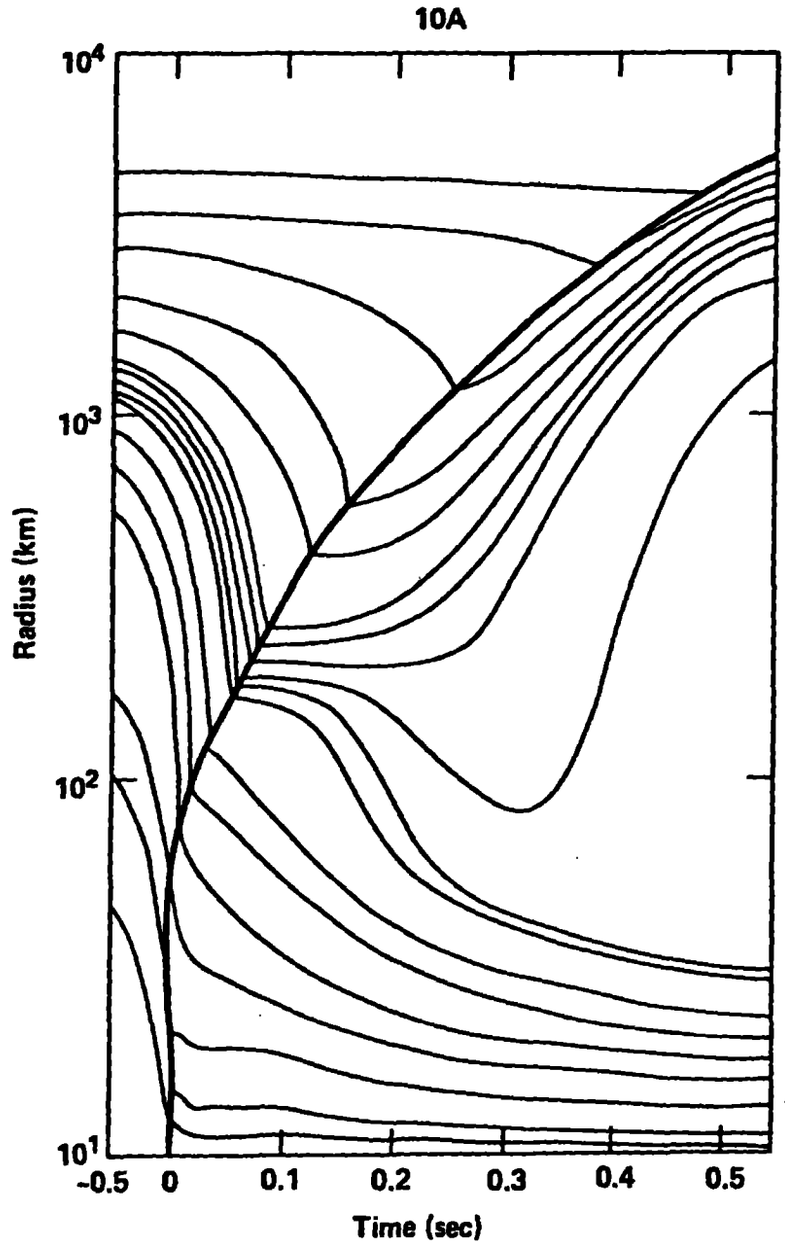

FIG. 8a

FIG 84

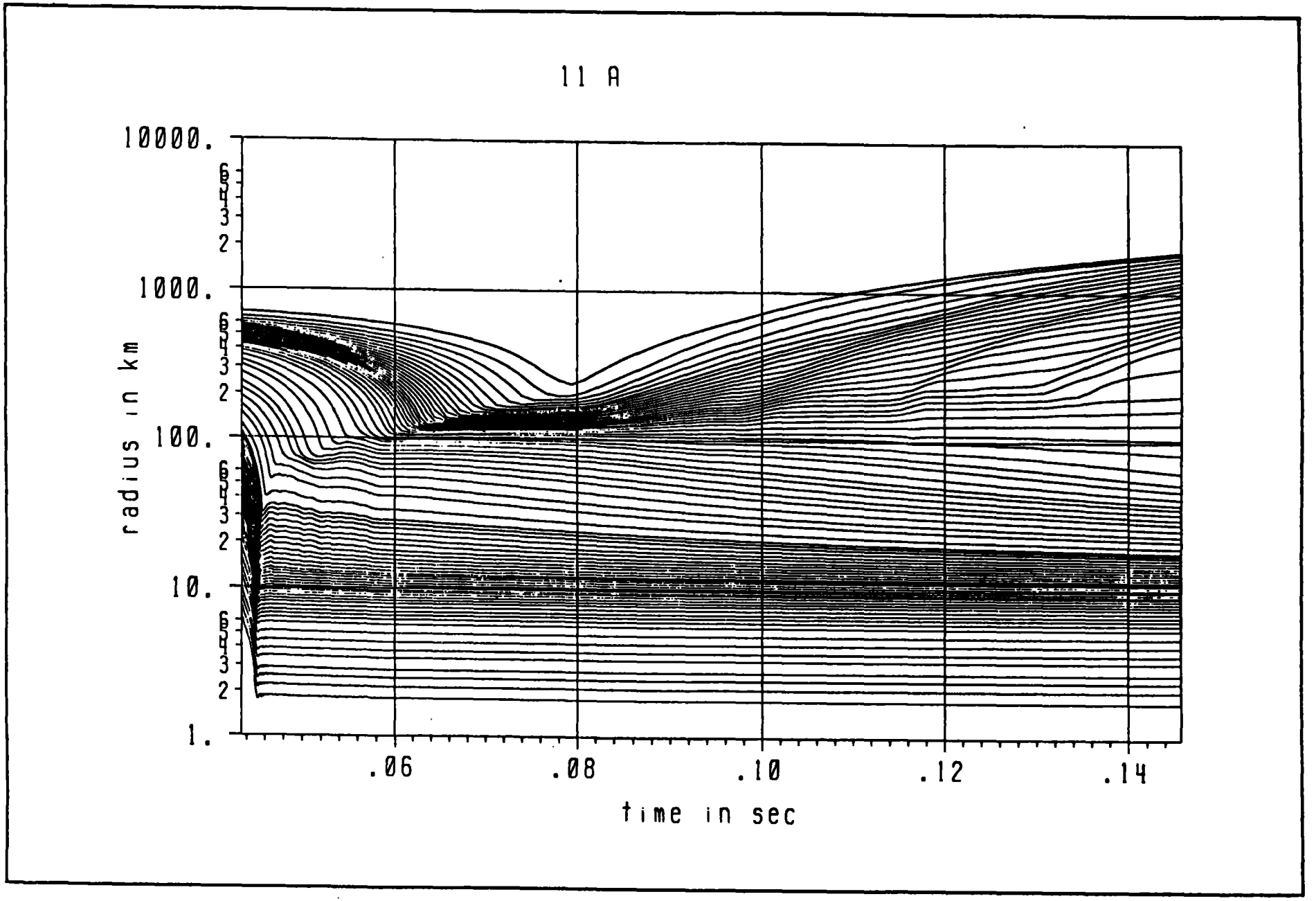

FIG. 8C

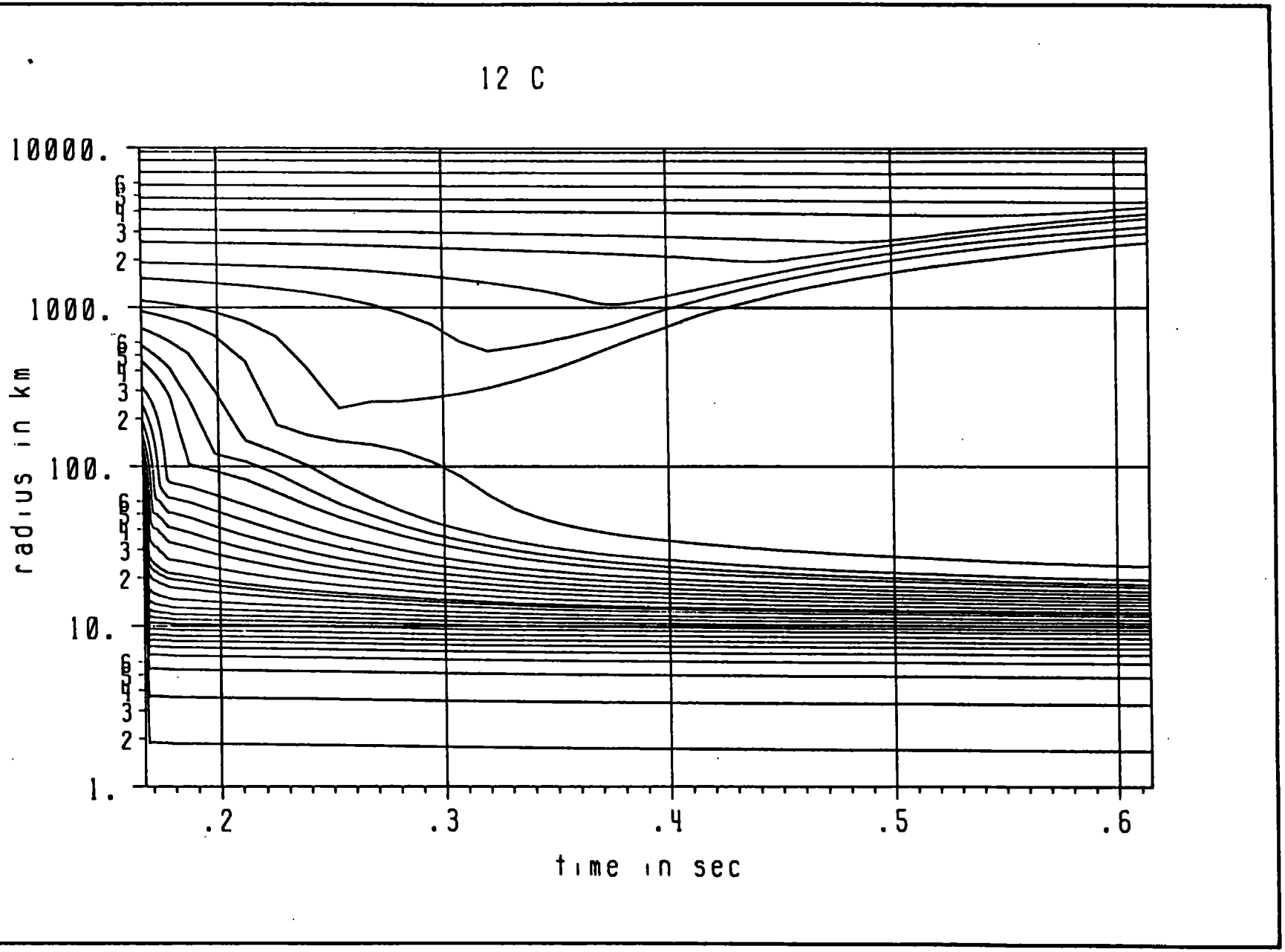

FIG. 8J

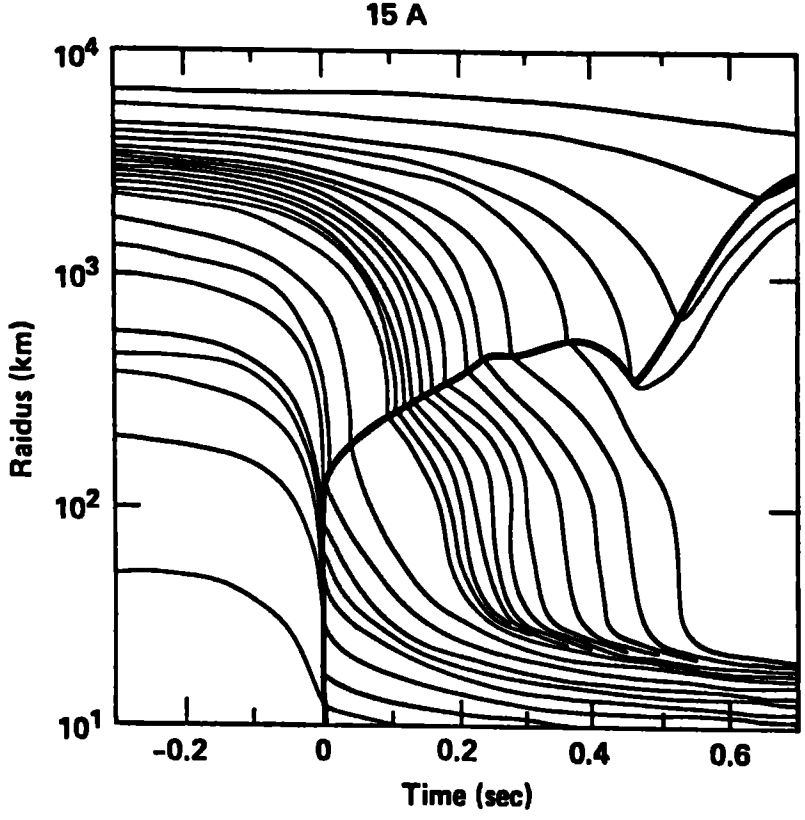

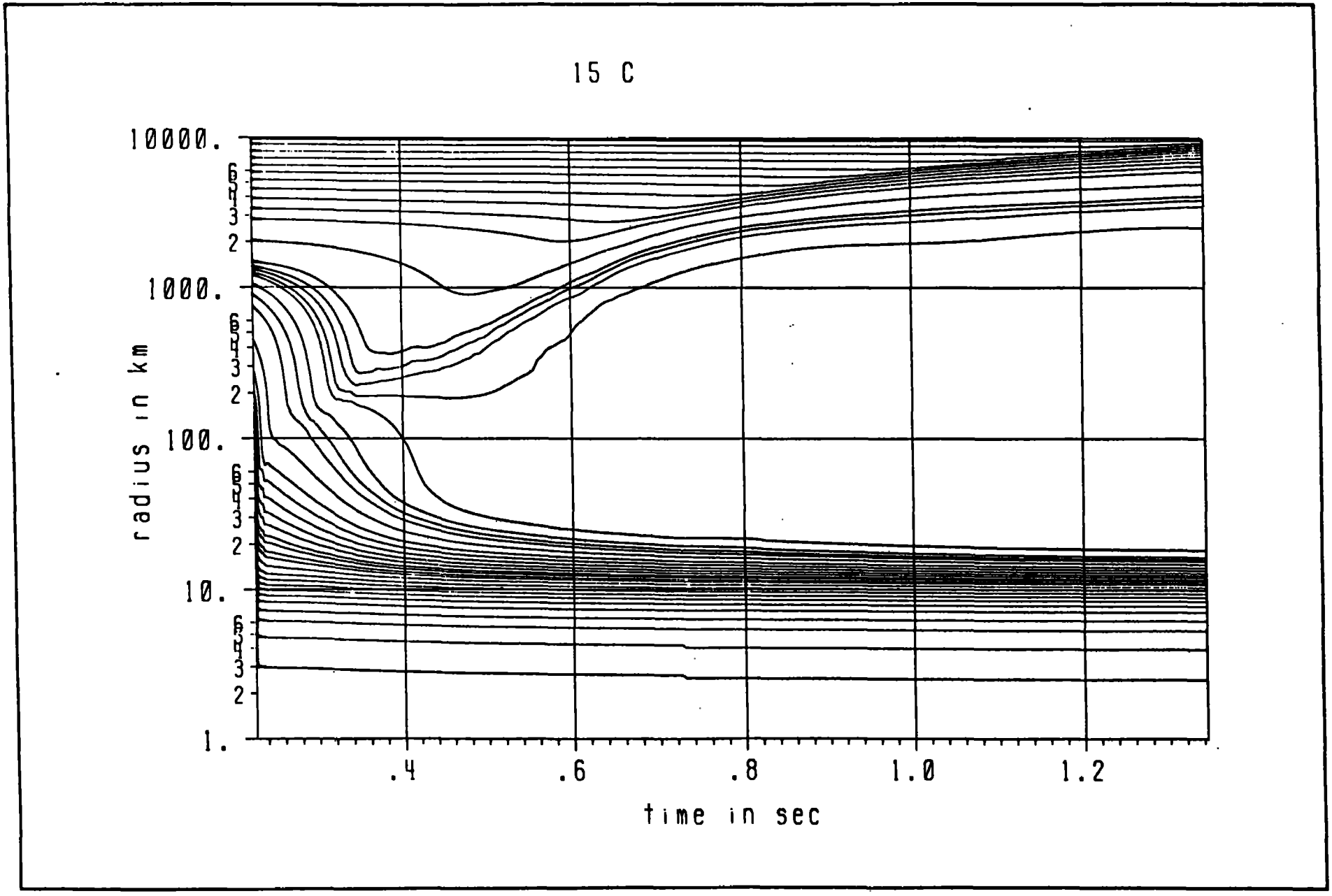

FIG. 8a

FIG 9f

Fig. 8a

25 B

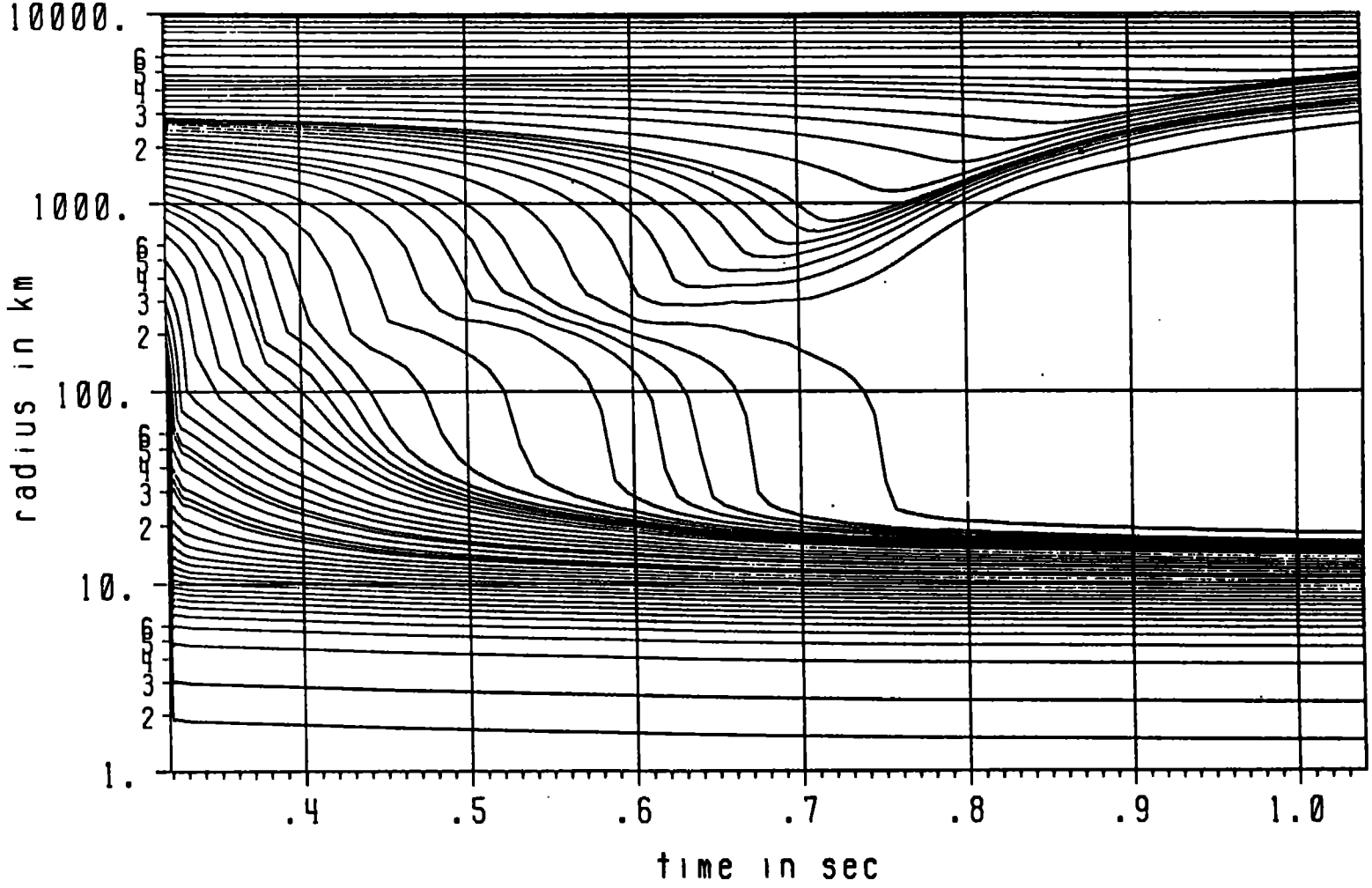

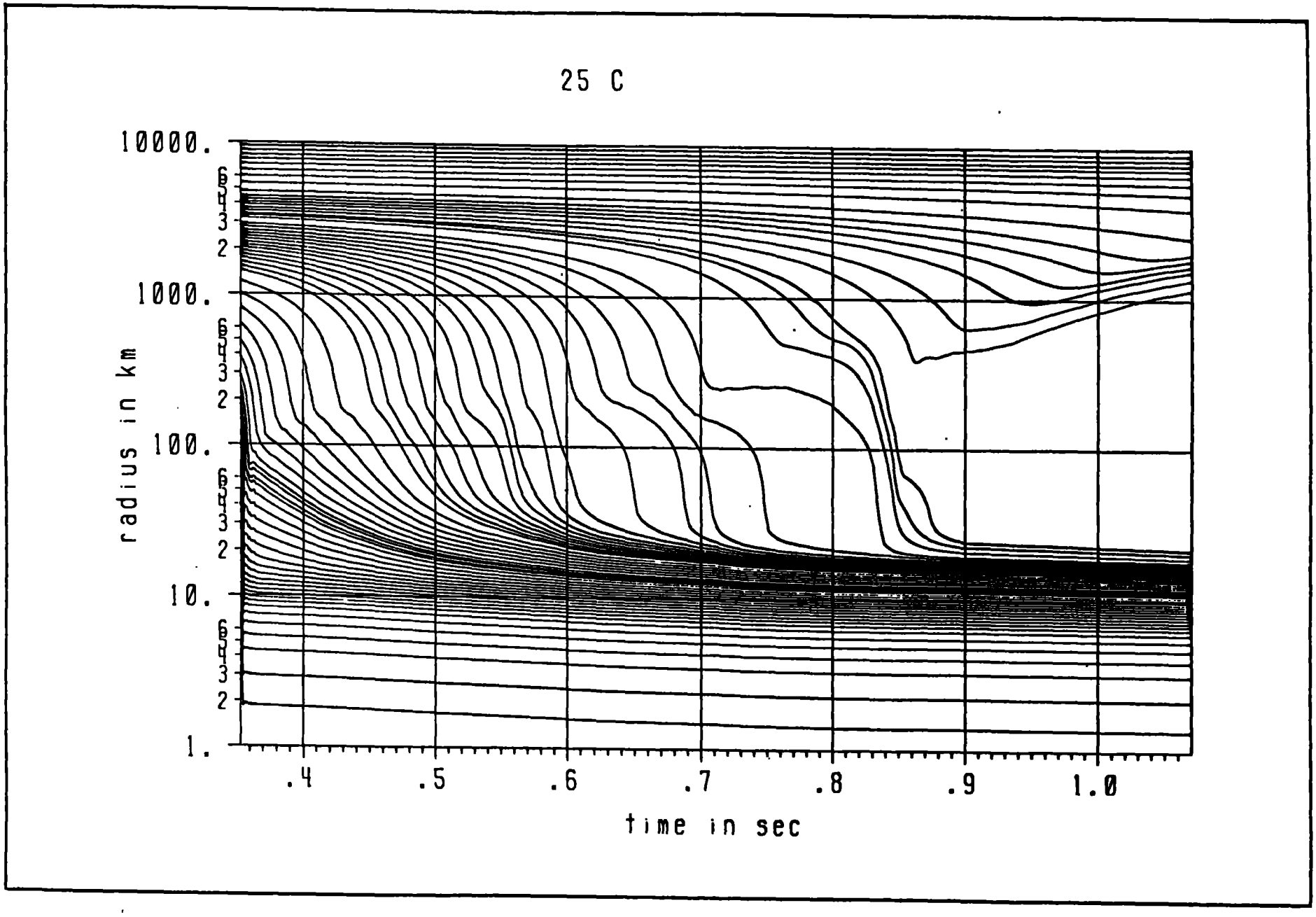

FIG. 8b

Fig 8:

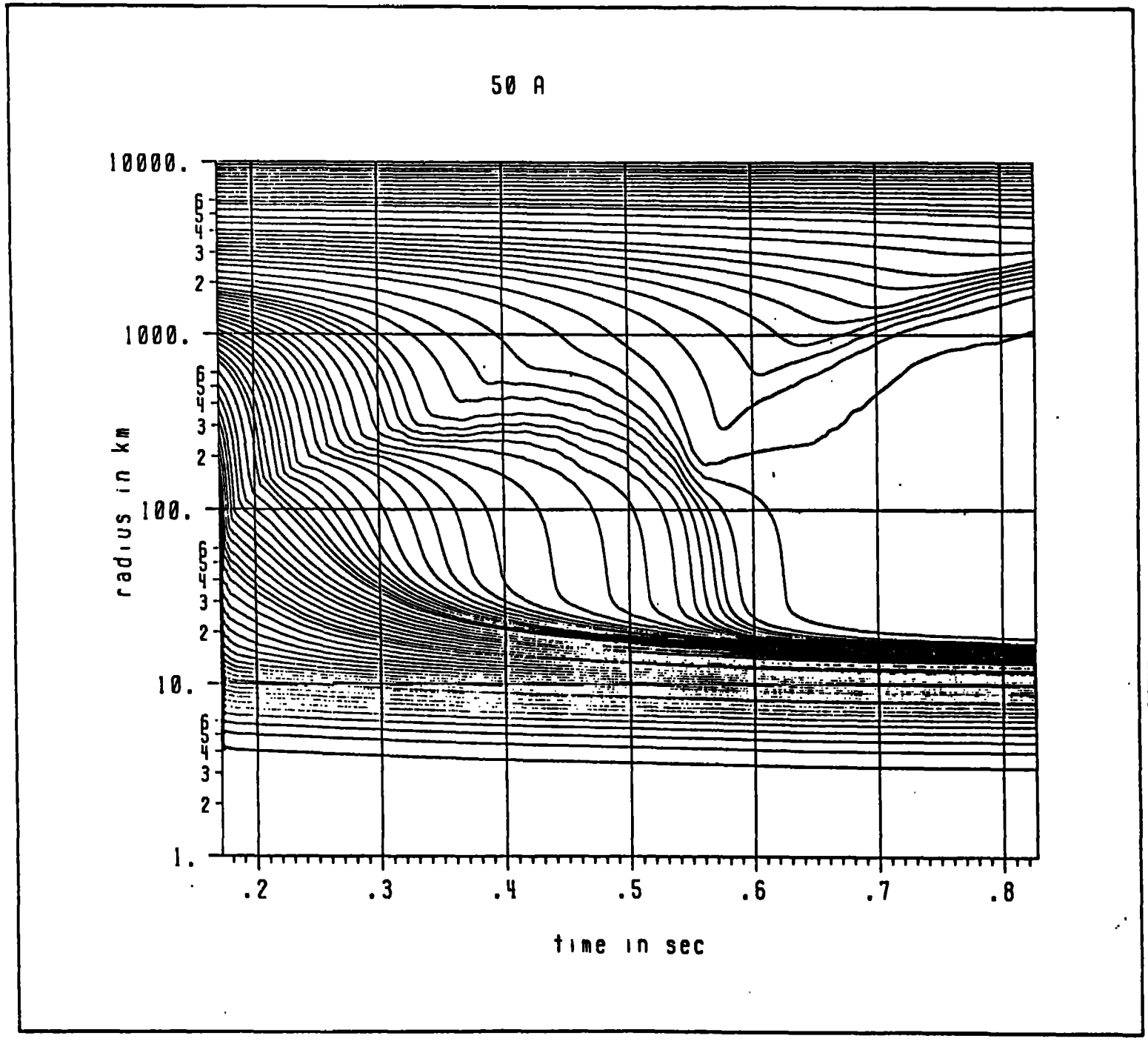

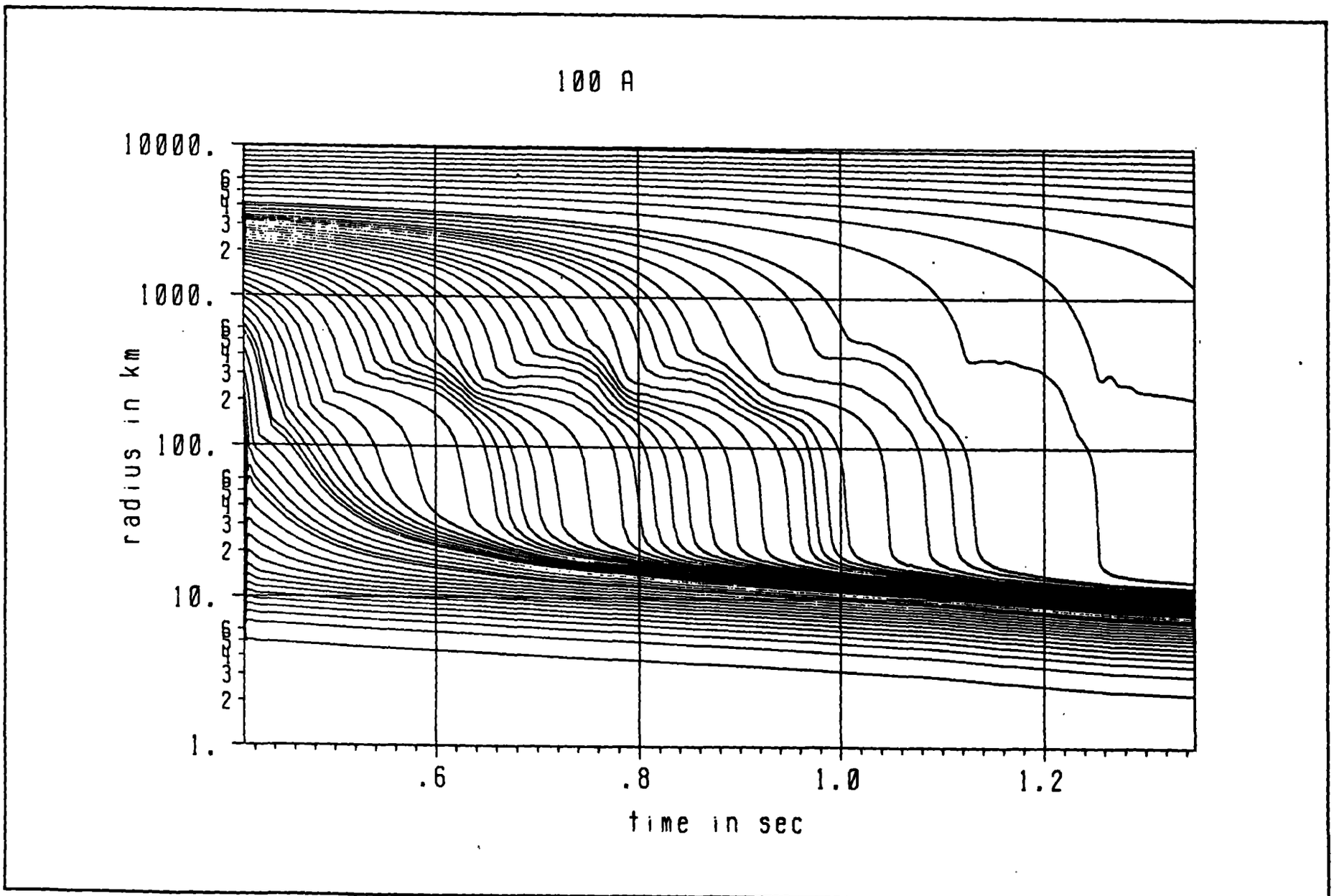

Fig. 8j

FIG 9

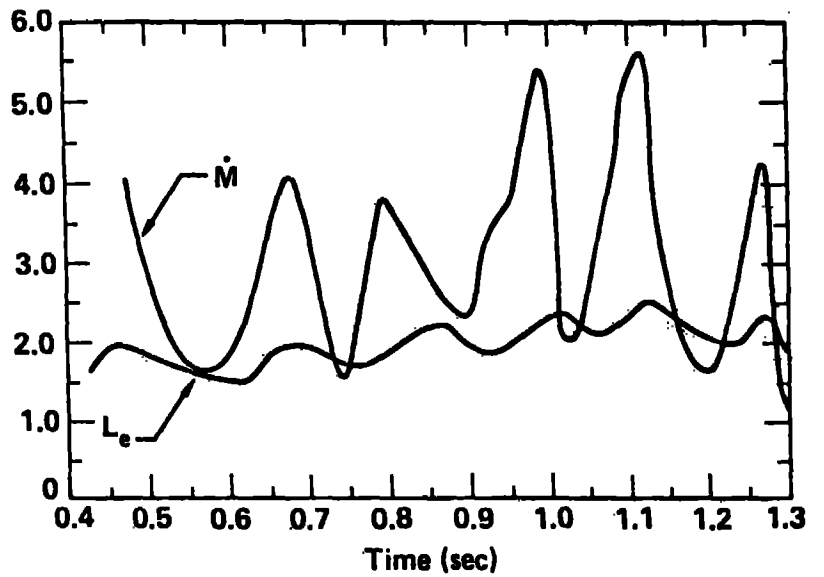

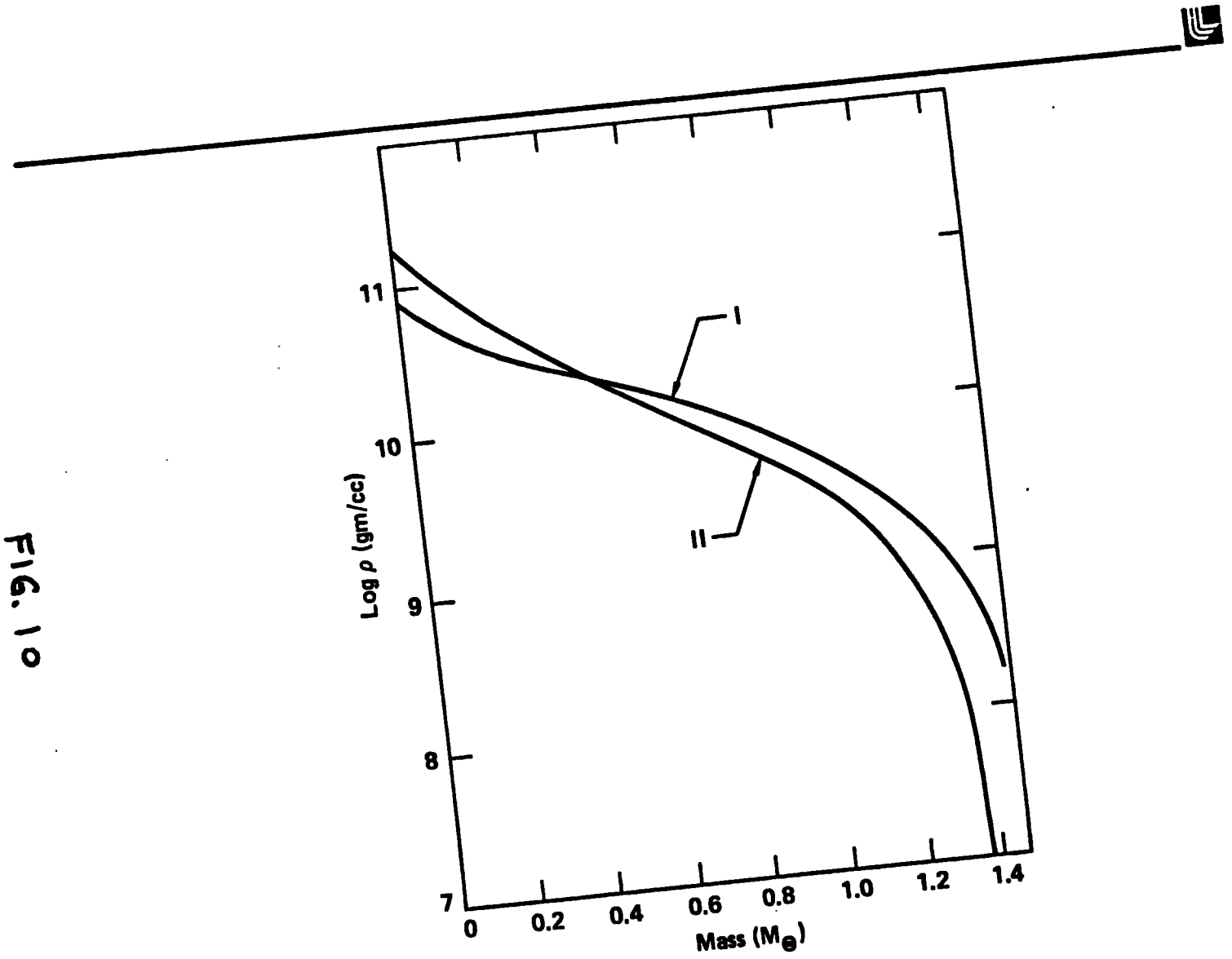

FIG. 10

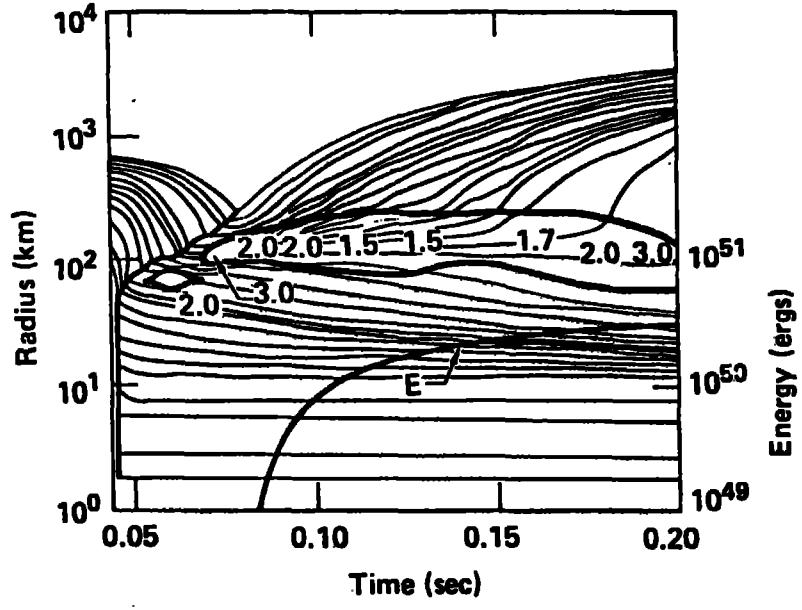
10^4
10^3
10^2
10^1
10^0
Radius (km)
2.0
2.0
1.5
1.5
1.7
2.0
3.0
2.0
3.0
E
10^{51}
10^{50}
10^{49}
Energy (ergs)
0.05
0.10
0.15
0.20
Time (sec)

FIG. 1

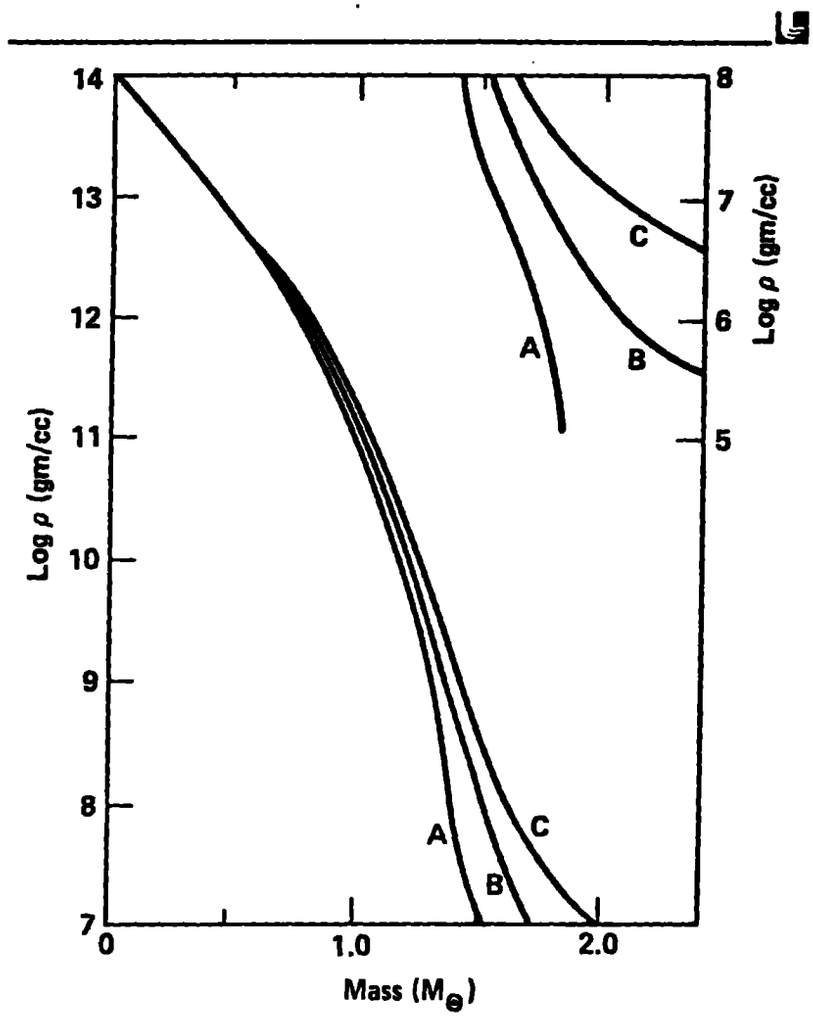
14
13
12
11
10
9
8
7
0
1.0
2.0
Mass ($M_\odot$)
Log ρ (gm/cc)
8
7
6
5
Log ρ (gm/cc)
A
B
C
A
B
C

FIG. 12

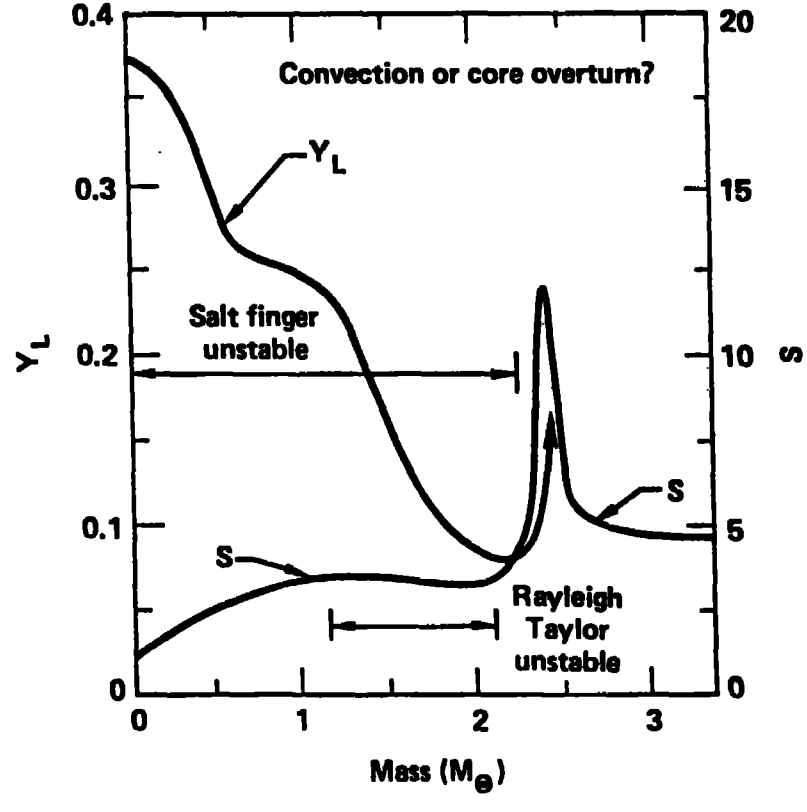
Convection or core overturn?
Y_L
Salt finger unstable
S
Rayleigh Taylor unstable
S
Y_L
0.4
0.3
0.2
0.1
0
20
15
10
5
0
0
1
2
3
Mass (M_Θ)

FIG. 13

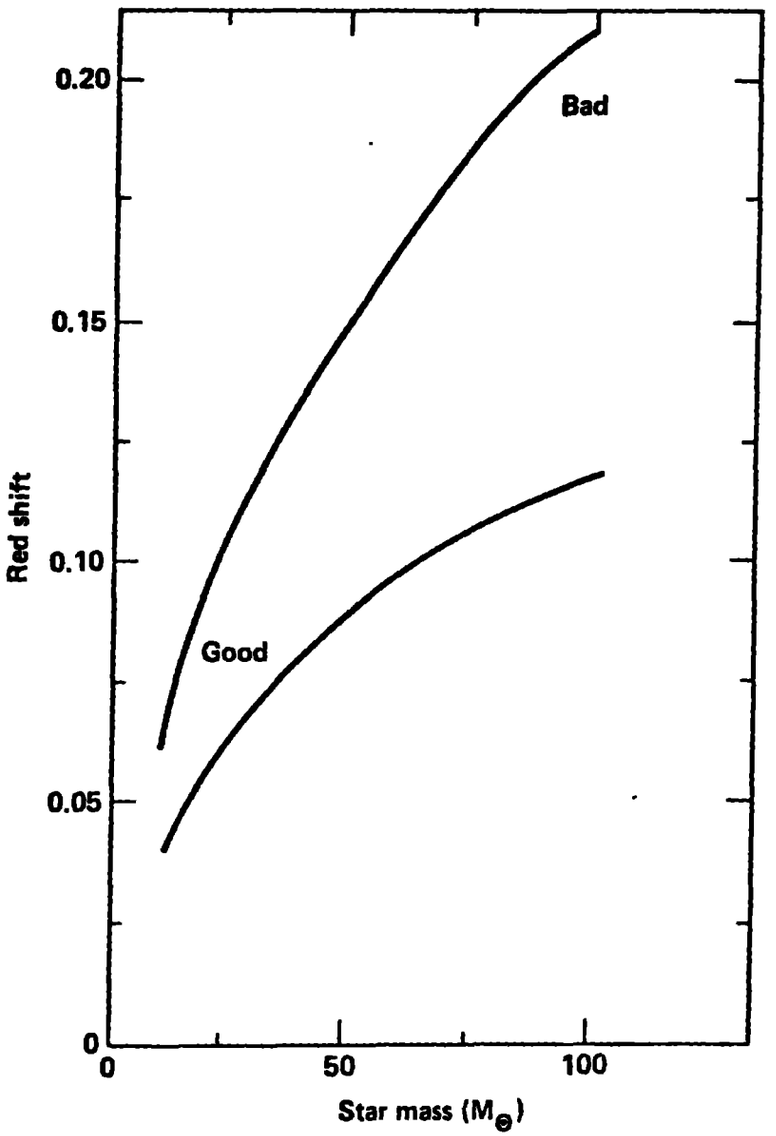

FIG. 14

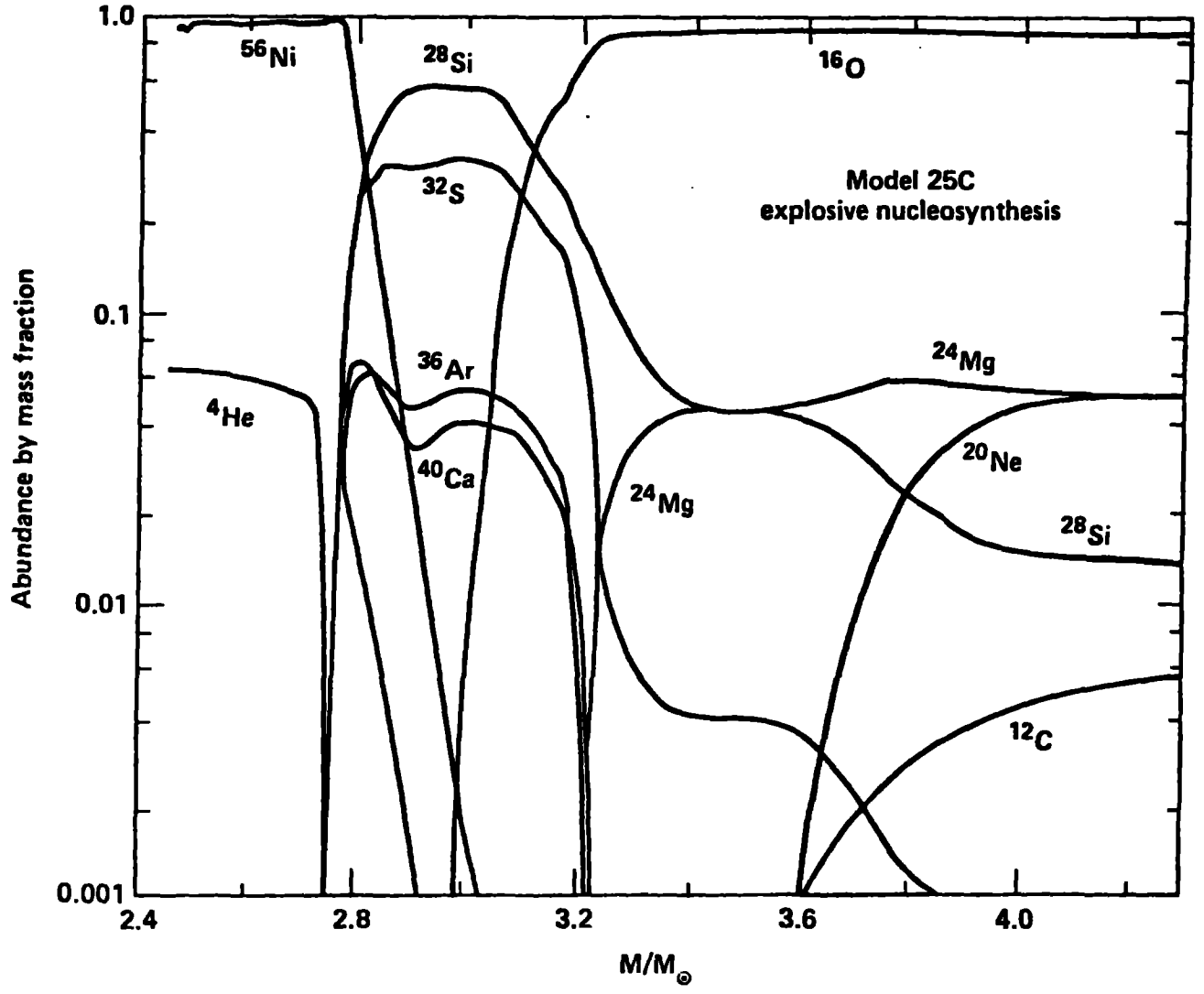
1.0
0.1
0.01
0.001
Abundance by mass fraction
2.4
2.8
3.2
3.6
4.0
M/M⊙
56Ni
28Si
16O
32S
Model 25C
explosive nucleosynthesis
36Ar
24Mg
4He
40Ca
24Mg
20Ne
28Si
12C

FIG. 15

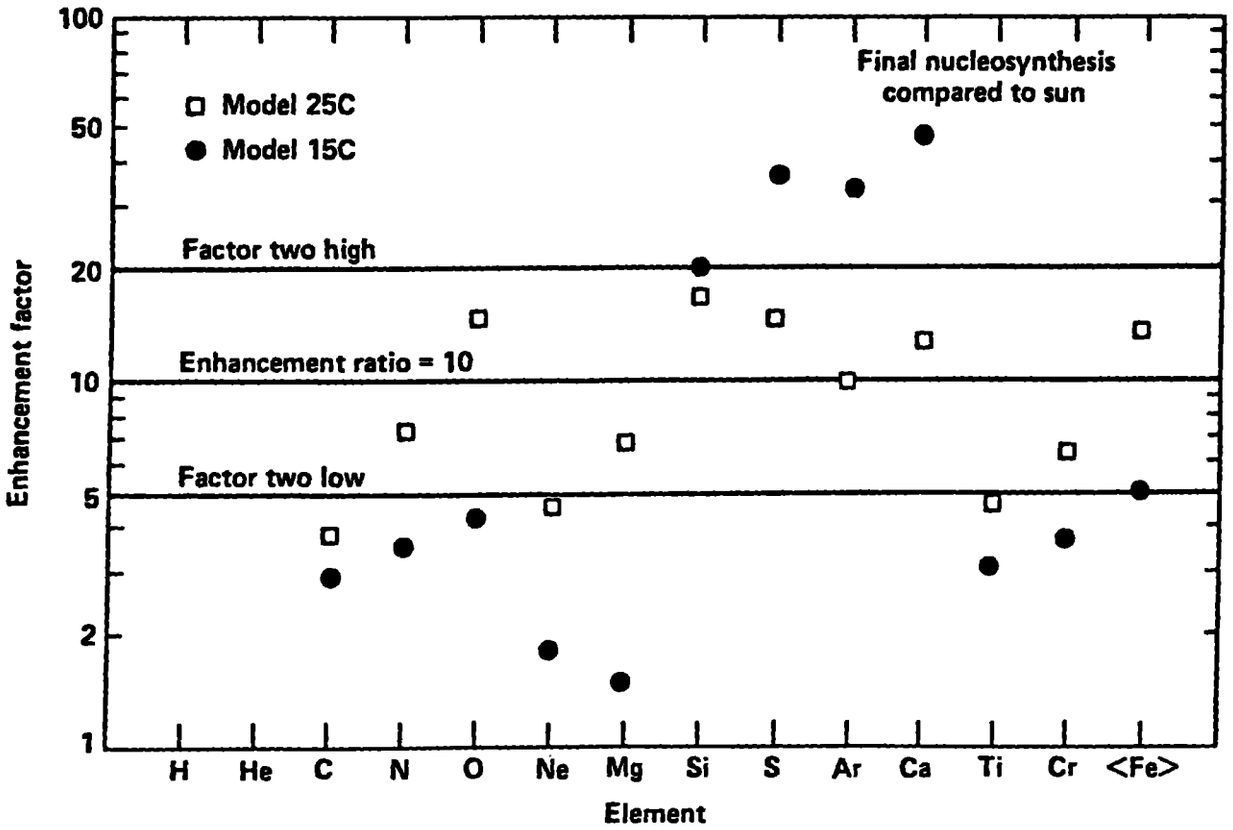
Final nucleosynthesis
compared to sun
Model 25C
Model 15C
Factor two high
Enhancement ratio = 10
Factor two low
Enhancement factor
100
50
20
10
5
2
1
H
He
C
N
O
Ne
Mg
Si
S
Ar
Ca
Ti
Cr
<Fe>
Element

FIG. 16

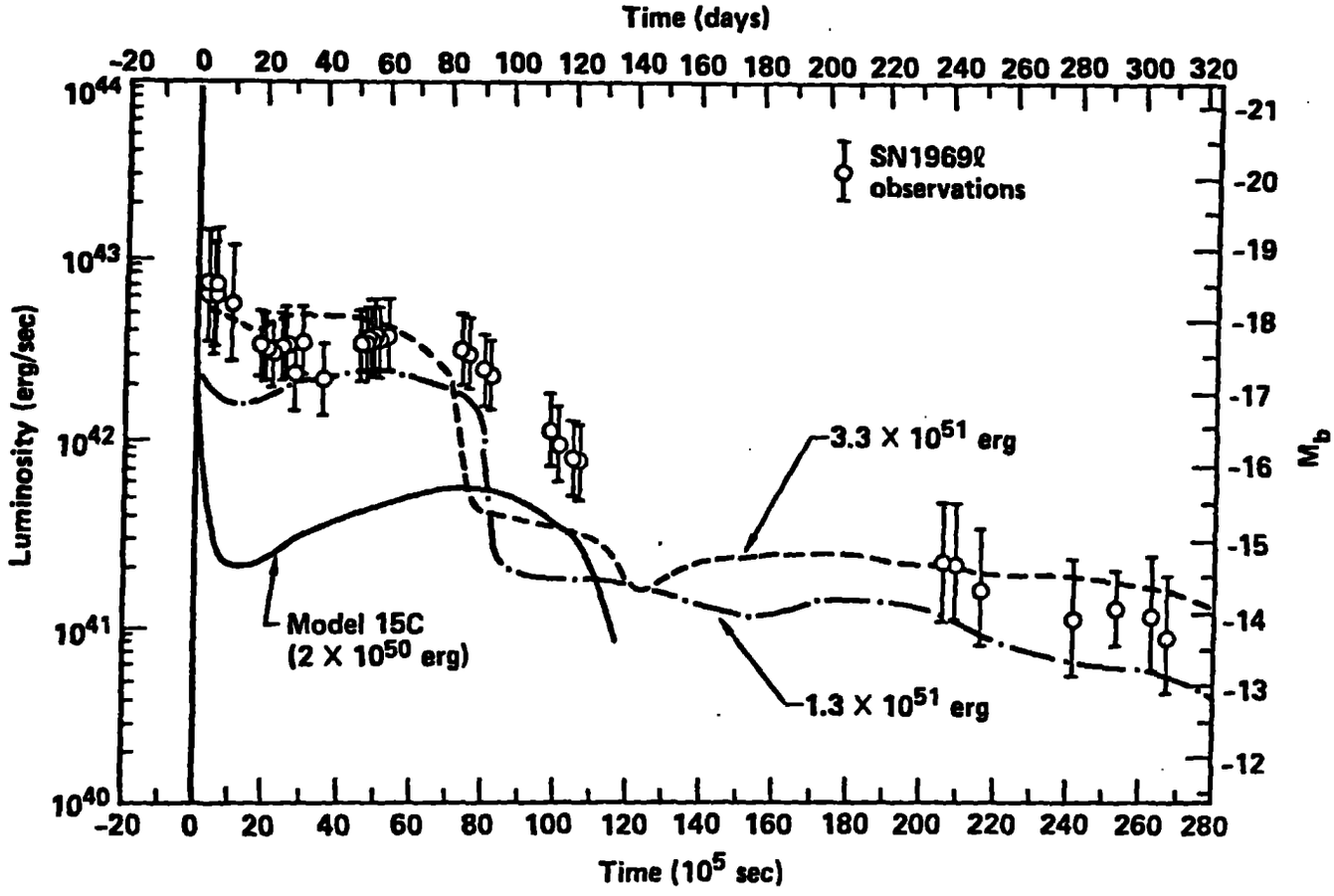
Time (days)
-20 0 20 40 60 80 100 120 140 160 180 200 220 240 260 280 300 320
10^{44}
10^{43}
10^{42}
10^{41}
10^{40}
Luminosity (erg/sec)
SN1969ℓ
observations
3.3 X 10^{51} erg
Model 15C
(2 X 10^{50} erg)
1.3 X 10^{51} erg
-21
-20
-19
-18
-17
-16
-15
-14
-13
-12
M_b
-20 0 20 40 60 80 100 120 140 160 180 200 220 240 260 280
Time (10^5 sec)

FIG. 17